Icarus **160**, 271–288 (2002)
doi:10.1006/icar.2002.6961

How Long-Lived Are the Hypothetical Trojan Populations of Saturn, Uranus, and Neptune?

D. Nesvorný and L. Dones

Department of Space Studies, Southwest Research Institute, 1050 Walnut Street, Suite 426, Boulder, Colorado 80302
E-mail: davidn@boulder.swri.edu

Received January 4, 2002; revised June 24, 2002

We investigate the possibility that fractions of the primordial populations at the triangular Lagrangian points of Saturn, Uranus, and Neptune have survived to the present and form (as yet unobserved) clusters of bodies coorbiting with these planets. Such leftovers would be analogs of the numerous objects (Trojans) leading and trailing the revolutions of Jupiter around the Sun. We focus on the dynamical stability of such populations over the age of the Solar System, assuming the current configuration of planets, and also discuss effects of the early radial migration of the outer planets. Our results suggest that, while Saturn's and Uranus' primordial Trojan populations should have been depleted by a factor of 100, Neptune may retain 50% of its original population of Trojans. A population of neptunian Trojans comparable to, or even larger than, Jupiter's Trojan population cannot be ruled out by existing observations. We compute the present-day sky densities of the hypothetical Trojans of the outer planets which can be used to guide observational surveys. Finally, we propose that the long-term instabilities that cause some jovian Trojans to escape the region of the Lagrange points at the present are due to three-body resonances. © 2002 Elsevier Science (USA)

Key Words: **Trojans; dynamics; resonances.**

1. INTRODUCTION

Jupiter's Trojans form two large groups of bodies leading (at L_4) and trailing (at L_5) the orbital revolutions of Jupiter around the Sun. The orbits of these bodies evolve on *tadpole* trajectories around the L_4 and L_5 points. The stability of the L_4 and L_5 orbits in the Sun–planet–small body system has been known since Lagrange, but only in the last decade (Holman and Wisdom 1993, Levison *et al.* 1997) has the stability of the Trojan population over the age of the Solar System been demonstrated by numerical integrations of a realistic model.

Numerical integrations by Innanen and Mikkola (1989) and Mikkola and Innanen (1992) showed that some tadpole orbits near the triangular Lagrange points of Saturn, Uranus, and Neptune were stable for 20 Myr. Holman and Wisdom (1993) determined the extent of the stable regions in detail, again on 20-Myr time scales. Holman and Wisdom confirmed Innanen and Mikkola's result that orbits very close to Saturn's L_4 (L_5) point are strongly unstable, so that the stable region contains a "hole." The only orbits near Saturn's L_4 (L_5) which are potentially stable over gigayear time scales are displaced from the exact position of the L_4 (L_5) point and oscillate about it with moderate amplitudes. Such stable orbits are nevertheless rare (Melita and Brunini 2001). Innanen and Mikkola (1989) and de la Barre *et al.* (1996) suggested that the instability near Saturn's Lagrange points was caused by the 5 : 2 near-resonance with Jupiter, while Marzari and Scholl (2000) found that two secular resonances were the main source of instability. Moreover, Saturn's Trojans could have been dynamically removed during the stage of early radial migration of the planets (Gomes 1998), and/or significantly reduced in number by mutual collisions (Marzari *et al.* 1996, 1997). For these reasons, it is unlikely that a *large* population of saturnian Trojans currently exists, and the lack of observational evidence for such a population is not surprising. Conversely, a small population of the primordial Saturn Trojans cannot be excluded (Melita and Brunini 2001).

Weissman and Levison (1997) numerically computed the stability of Neptune's Trojans, initially placed on orbits near the invariable plane, over 4 Gyr. The tadpole orbits started with small proper eccentricities ($\lesssim 0.05$) were shown to be generally stable unless their libration amplitudes (i.e., the full angular extent of a tadpole orbit) exceeded 60°. The stability of Uranus' and Neptune's *nonplanar* Trojans on gigayear time scales is unknown. It is of interest to determine whether or not such populations may be ruled out by dynamical instabilities. In the latter case, Trojans of Uranus and Neptune may be discovered in the future, and if not, some primordial mechanism must have been responsible for their absence. This is in our opinion an interesting logical chain, which can eventually set some constraints on the formation of Uranus and Neptune themselves.

The main objective of this work is to understand the dynamical evolution and stability of the hypothetical Trojans of Saturn, Uranus, and Neptune. We concentrate on the primordial bodies, permanently residing near the L_4 (L_5) point since the formation of the outer planets, and do not investigate the possibility that some ecliptic comets became temporarily captured there (Everhart 1973). Temporary captures of Near-Earth Objects have been shown to produce the discovered coorbitals of Mars (e.g.,

0019-1035/02 $35.00
© 2002 Elsevier Science (USA)
All rights reserved.

(5261) Eureka—Mikkola *et al.* 1994) and Earth (e.g., (3753) Cruithne—Wiegert *et al.* 1997). See Christou (2000) for a recent review.

We proceed in two steps: (i) we run short-time ($\approx$10–100 Myr) and high-resolution surveys (thousands of test bodies) of the maximum Lyapunov characteristic exponents (LCE-Section 2), and (ii) we numerically integrate a few hundred selected orbits over 4 Gyr (Section 4). The first simulation allows us to understand the dynamical behavior of the outer planets' Trojans and to select the potentially stable orbits for the second simulation. We then use (ii) for the computation of the sky densities of the hypothetical Trojan populations and discuss the efficiency of past observational surveys and the optimal strategy of future surveys (Sections 5 and 6).

Section 3 is devoted to some interpretations related to the structure of regular and chaotic trajectories in the coorbital regions. In Section 3, we also study effects of the primordial migration of the outer planets on their Trojans.

We adopt the usual notation, denoting by a, e, i, ϖ, ω, Ω, and λ the semimajor axis, eccentricity, inclination to the invariable plane, perihelion longitude and argument, node longitude, and mean longitude of a small body, respectively, and by a_j, e_j, i_j, ϖ_j, ω_j, Ω_j, and λ_j the same elements of the jth planet ($j = 5, 6, 7, 8$ for Jupiter, Saturn, Uranus, and Neptune, respectively).

Observational and dynamical overviews of jovian Trojans can be found in Shoemaker *et al.* (1989) and Marzari *et al.* (2002).

2. SHORT-TIME, HIGH-RESOLUTION SURVEYS

We numerically integrated the orbits of the Sun, the four outer planets (Jupiter, Saturn, Uranus, and Neptune), and test bodies. While the planets gravitationally interacted among themselves and on the test bodies, each test body was assumed massless with no effect on other bodies in the integration. The equations of motion were numerically solved by *Snail*. This program implements the symmetric multistep integrator (Quinlan and Tremaine 1990).

The initial coordinates and velocities of the planets were obtained from the JPL DE-405 ephemeris (http://ssd.jpl.nasa.gov/eph_info.html) on JED 2451544.5 (1/1/2000). They were rotated to the invariable plane determined by the total angular momentum of the Solar System. The coordinates and velocities of the outer planets were corrected for the barycenter of the inner Solar System. The masses of the inner planets were then added to the mass of the Sun.

The test bodies were initially placed near the leading Lagrangian points L_4 of the outer planets. According to our tests, the L_4 and L_5 points show no asymmetry concerning the dynamics and stability of orbits around them. For this reason, we chose to sample only the orbits around the L_4 point, expecting the dynamics around the L_5 point to be a mirror image of the studied sample. We initially set $\sigma \equiv \lambda - \lambda_j = \sigma_c(e)$, where $\sigma_c(e)$ is the center of the tadpole orbits. This center is near 60° for $e \approx 0$ and has larger values for larger e (Namouni 1999). This choice ensures that our set of initial orbital elements samples the tadpole orbits of all amplitudes.

Motivated by our preliminary study of the secular dynamics at the outer planets' L_4 points (Fig. 1), we initially chose $\varpi - \varpi_j = 60°$ for the test particles at Jupiter's and Saturn's L_4 points and $\varpi - \varpi_j = 240°$ for those at Uranus' and Neptune's L_4 points. This choice ensured that our set sampled the orbits with different secular evolutions, including those for which $\varpi - \varpi_j$ oscillates about a fixed value (Fig. 1). Moreover, we assumed $\Omega - \Omega_j = 0$.

This choice of angular variables and the fine sampling of the semimajor axis and eccentricity (to be discussed in the following) ensured a coverage of the coorbital region which is more representative than the choice usually made (e.g., Holman and Wisdom 1993, Melita and Brunini 2001). Unlike the previous works, we accounted for initially eccentric orbits and did not "double" the result by sampling equal-amplitude orbits several times.

We used time steps of 20/20, 40/40, 40/80, and 40/160 days in the runs with Jupiter's, Saturn's, Uranus', and Neptune's Trojans, respectively, where the first number is the time step used for the planets and the second one is the time step used for the test bodies. The time step for the integration was always less than 1% of the shortest orbital period, so that the integration method would not create spurious chaotic regions associated with low-order resonances between the time step and the dynamical frequencies (Wisdom and Holman 1992). The total simulation times were 7.7, 18.6, 39.4, and 87.1 Myr. A test body was removed from the simulation if it was released from the coorbital space of a planet. Such a body is easily recognized because its orbit rapidly evolves to $a \neq a_j$ by encounters with planets, which can be checked by its heliocentric distance. The variational equations were solved by the same method and the maximum LCE was computed for each surviving test body (Fig. 2). Nonzero values of the maximum LCE are indicators of chaos (Oseledec 1968, Benettin *et al.* 1976; see also Morbidelli and Nesvorný (1999) for numerical examples related to small-body dynamics).

The initial a and e of test bodies were chosen to have a good coverage of interesting orbits. The spacing was such that there were 100 test bodies within the semimajor axis range shown in the figures per one value of e and a spacing in eccentricity $\Delta e = 0.01$. For bodies on tadpole orbits with Jupiter, we initially set $i = 10°$; for the other planets, we set $i = 0°$ with respect to the invariable plane. To span the inclination distribution of the observed Trojans, whose mean inclination is $\approx$18°, we also ran an additional integration for Jupiter with $i = 30°$. Initially near-planar orbits of test bodies for the other planets should correspond to locations where stability is expected.

We sample by initial orbital elements only a small part of the coorbital region. This can be seen from Fig. 3, where the full extent of the coorbital region is shown. Different lines in Fig. 3 delimit the occurrence of various types of coorbital motion; for example, the lines denoted by (2) and (3) show the limits of the

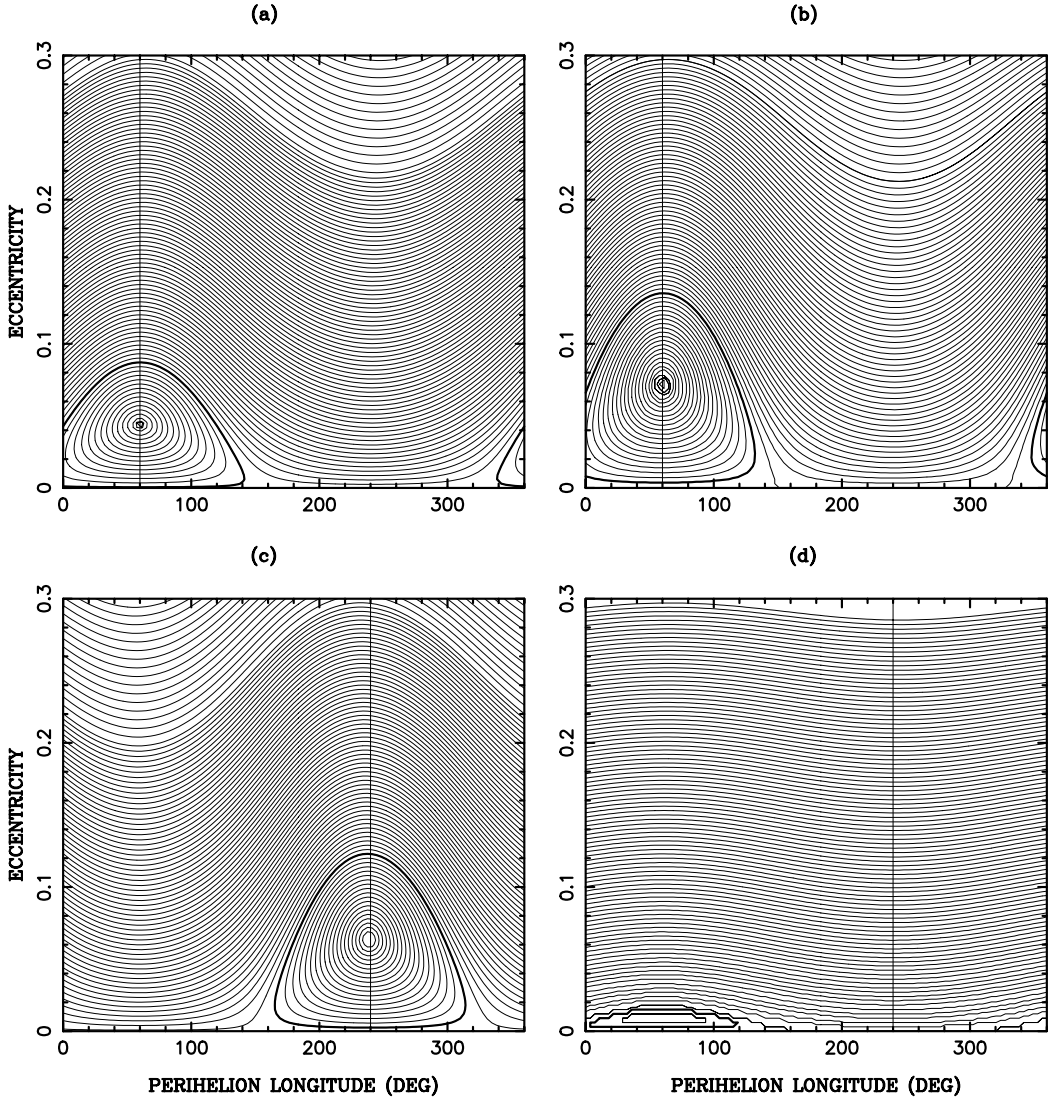

FIG. 1. Secular evolution of $(e, \varpi - \varpi_j)$ of the low-amplitude tadpole orbits at the L_4 points of Jupiter (a), Saturn (b), Uranus (c), and Neptune (d). These plots have been computed analytically by the method described in Nesvorný *et al.* (2002). In each case, we account for the precession of the planet's elliptic orbit given by the leading term in the Fourier series of $e_j \cos \varpi_j$ (Bretagnon and Simon 1990). Using the Hamiltonian formulation, we numerically average the equations of motion over the short-period terms. The averaged Hamiltonian generated by this procedure has two degrees of freedom. The two angles that appear in the averaged Hamiltonian are $\sigma = \lambda - \lambda_j$ and $\varpi - \varpi_j$. With $\sigma = \sigma_c$, the Hamiltonian is reduced to one degree of freedom. The level curves of this Hamiltonian are trajectories of $(e, \varpi - \varpi_j)$ shown in the figure. For Uranus' L_4, the stable point of $\varpi - \varpi_7$ is at $\approx 240°$. The bold lines delimit the islands associated with the stable points. The vertical lines show our choice of the initial $\varpi - \varpi_j$.

tadpole and horseshoe domains, respectively. The horseshoe and large-amplitude tadpole orbits not sampled in Fig. 2 are strongly unstable. Such orbits cannot host any long-lived population of bodies.

We have checked that, for the range of masses of the outer planets (roughly 10^{-3}–10^{-4} $M_\odot$), the horseshoe orbits are unstable on short time spans in the planar, circular three-body model (Fig. 4). Thus, the secular resonances do not cause the instabilities of the horseshoe orbits. The instabilities of horseshoe orbits probably occur due to the overlapping of the coorbital region with $N/(N-1)$ and $(N-1)/N$ mean motion resonances with the planet, where N is a sufficiently large integer. We have found that, for $N \geq 5$, such resonances overlap with the horseshoe domain. It is known that overlapping of mean motion resonances generates large-scale chaos in the vicinity of a planet (Wisdom 1980).

In the case of Jupiter (Fig. 2a), our survey confirms a large, practically regular nucleus of tadpole orbits found by previous studies (Holman and Wisdom 1993, Levison *et al.* 1997). The Trojan asteroids are mostly located in this region, usually having libration amplitudes $\lesssim 40°$. From dynamical features identified by the survey, we note a structure of parallel, almost vertical ridges of larger LCE symmetrically placed around 5.2 AU and forming a V-shaped pattern (marked by dashed lines on the

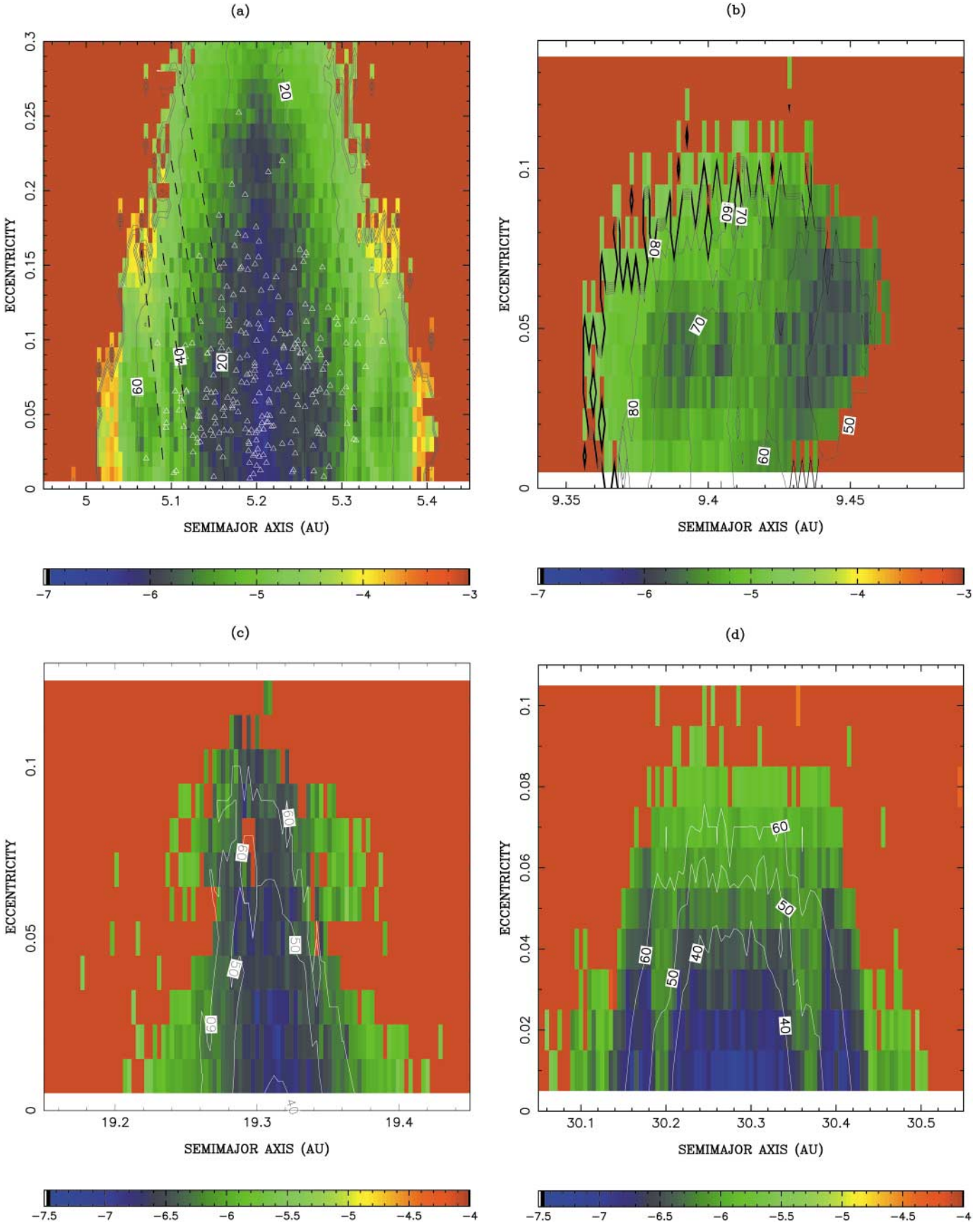
(a)
(b)
(c)
(d)
ECCENTRICITY
SEMIMAJOR AXIS (AU)

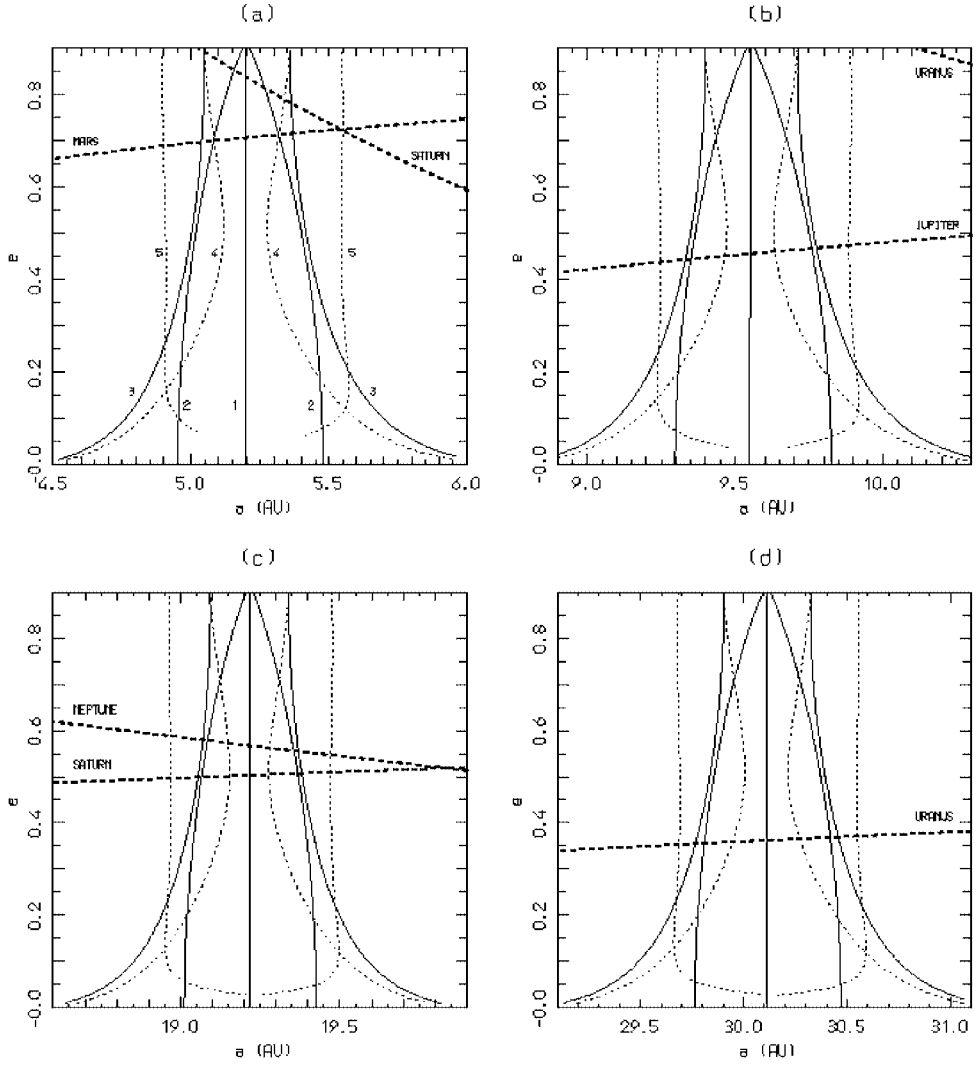

FIG. 3. The structure of the coorbital regions of the outer planets: (a) Jupiter, (b) Saturn, (c) Uranus, and (d) Neptune (from Nesvorný *et al.* 2002). This figure shows the center (1) and limits of tadpole orbits (2) and the limits of horseshoe orbits at $\lambda - \lambda_j = \sigma_c(e)$ (3) and at $\lambda - \lambda_j = 0$ (4). The line (5) shows the limits of domain of the distant retrograde satellites (e.g., Namouni 1999). Orbits above the bold dashed lines are planet crossing. Positions of the tadpole center and limits of different domains were computed analytically. Note that the initial conditions of our short-time, high-resolution surveys (Fig. 2) cover only small rectangles in (a, e) space, corresponding to small-e tadpole orbits.

side of small a). One of these features descends to $e = 0$ at $a = 5.17$ and 5.25 AU. These ridges may correspond to the perihelion-secular or three-body resonances, both having about the same shape in (a, e) space. The perihelion resonances are, however, hardly present; due to the relatively fast evolution of ϖ at $i = 10°$ (∼350–400 arcsec/year, prograde), such resonances are of very high order, and consequently they must be very weak. The three-body resonances are probably a better guess, because the period of resonant oscillations of Jupiter's Trojans is commensurable with the period of $\lambda_5 - 2\lambda_6$.

We have investigated this problem in detail and found several reasons to believe that ridges of higher LCE are due to the

FIG. 2. The $\log_{10}$ of the maximum LCE for orbits near the Lagrangian L_4 points of Jupiter (a), Saturn (b), Uranus (c), and Neptune (d). Here, the centers of tadpole orbits are at 5.2, 9.55, 19.32, and 30.27 AU in terms of the initial semimajor axis. These values correspond to zero-amplitude tadpole orbits with the mean semimajor axes of 5.2, 9.55, 19.22, and 30.1 AU, respectively (see Fig. 3). The plots are nearly symmetric with respect to these semimajor axes due to our choice of the initial $\lambda - \lambda_j$. The red color denotes the strongly chaotic orbits which escape from the coorbital space in the integration time span. The blue color denotes regular and weakly chaotic orbits. In (a), the known Trojan asteroids associated with Jupiter's L_4 point are shown (triangles). The dashed lines in (a) denote places of nearly constant libration frequency of σ, where three-body resonances occur. In all panels, the libration amplitude of tadpole orbits is shown by contour plots (numbers are in degrees). Note that for Saturn, most of the low-amplitude tadpole orbits near 9.55 AU are unstable on the integration time span.

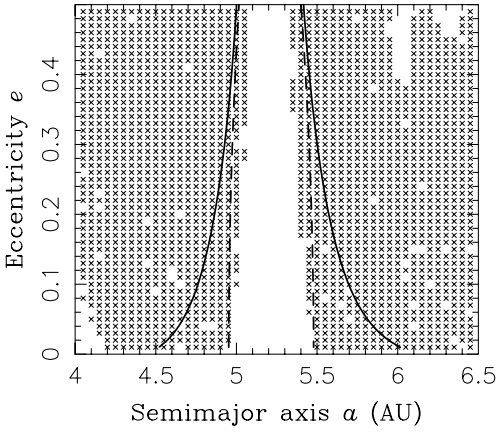

FIG. 4. The stable (void) and unstable (×) test orbits in the planar, circular, restricted three-body model with Jupiter at 5.205 AU. The dashed and the full lines show the limits of the tadpole and horseshoe regions for $\sigma = \sigma_c(e)$, respectively. The test orbits were started with $\sigma = \sigma_c(e)$ and $\varpi = 0$ and were numerically integrated for 10^6 years or until they collided with Jupiter. This figure shows that the horseshoe orbits of Jupiter are unstable in this simple model. The same holds for Saturn, Uranus, and Neptune.

three-body resonances with resonant angles:

$$5(\lambda - \lambda_5) - 2(\lambda_5 - 2\lambda_6) + k\varpi + k_5\varpi_5 + k_6\varpi_6, \qquad (1)$$

where $k + k_5 + k_6 = -2$. Since $\dot{\varpi} \gg g_6 > g_5$, where $\dot{\varpi}$, g_6, and g_5 are the Trojan's and planetary frequencies, such resonances occur in tight multiplets where k is fixed and k_5, k_6 range over the values dictated by the d'Alembert rules. The resonant multiplets occur at places of higher LCE. The dashed lines in Fig. 2a correspond to $k = 2, 0, -2$, and -4, from left to right, respectively. These resonant locations have been computed by the Fourier analysis of the integration output determining all frequencies involved in resonant combinations (Eq. (1)) on a grid in (a, e).

The suggested resonances are of the fifth power in the $\lambda - \lambda_5$ amplitude (A_σ) and of low order in eccentricities and inclinations. Thus, they must grow in importance at moderate to large A_σ, giving that location an appearance of gradually increasing orbital instabilities. Such a situation is similar to what happens in some mean motion resonances in the Kuiper Belt (Nesvorný and Roig 2000). We thus believe, although a detailed computation of the strengths of the individual multiplets is yet to be done, that the three-body resonances are the main source of the marginally unstable region at $\gtrsim 40°$ resonant angle amplitudes found by Levison *et al.* (1997). In this region, mostly denoted in green in Fig. 2a (LCE $\approx 10^{-5}$ year^{-1}), the number of Jupiter's Trojans drops significantly.

The survey with initial $i = 30°$ revealed structures similar to Fig. 2a (where $i = 10°$), only this time the stable region around the L_4 point shrinks faster with increasing e. This is reflected in the population of real Trojans, since few observed objects with $i \gtrsim 20°$ have $e \gtrsim 0.15$.

The case of Saturn is particularly interesting because, as anticipated from previous studies, the tadpole trajectories near L_4 are strongly unstable (Fig. 2b). In fact, all orbits started at $9.46 < a < 9.64$ AU escape in less than a few million years. We show in Fig. 2b only the interesting region at 50–85° amplitudes, where some orbits survive over longer time intervals. It has been suggested that the instability at small A_σ at Saturn's L_4 and L_5 points (Holman and Wisdom 1993) occurs due to the so-called Great Inequality, the 5 : 2 near-resonance between Jupiter and Saturn (Innanen and Mikkola 1989, de la Barre *et al.* 1996). We scrutinize this possibility in the next section. Our additional run with nonzero inclinations of test bodies showed that the niche of $\gtrsim$10-Myr stability at Saturn's L_4 seen in Fig. 2b shrinks by a factor of 2–3 in a at $i = 25°$.

Uranus' low-LCE tadpole orbits are limited to small amplitudes ($\lesssim 60°$) and $e < 0.1$ (Fig. 2c). In the case of Neptune (Fig. 2d), the limiting eccentricity is even smaller. Conversely, the semimajor axis extent of Neptune's low-LCE orbits is larger than in the case of Uranus. The prominent feature seen in Fig. 2d at 30.2 and 30.37 AU is the secular resonance $s = s_8$ (the ν_{18} secular resonance), where s and s_8 are the nodal frequency of the small body and $\dot{\varpi}_8$, respectively.

3. STABILITY OF SATURNIAN TROJANS AND THE GREAT INEQUALITY

The Great Inequality is a historical name for the quasi-resonance between the orbital motions of Jupiter and Saturn. Indeed, the angle $\phi_{JS} = 2\lambda_5 - 5\lambda_6$ varies much more slowly than the orbital motion: It circulates with a period of $\approx$880 years. This means that Saturn moves very near the exterior 2 : 5 mean motion resonance (MMR) with Jupiter. Consequently, Saturn's hypothetical Trojans should also be affected by this resonance.

To study this case, we adopt a simple "bi-circular" model assuming both planets to move on coplanar, circular, and non-interacting orbits. The inclinations of small bodies are assumed to be 0. The equations of motion then contain only four angles: λ, ϖ, λ_5, and λ_6. Consequently, the model possesses four degrees of freedom.

The next step we take is to average over short-period terms and to retain solely the resonant combinations $\lambda - \lambda_{j_1}$ and $k\lambda - k_{j_2}\lambda_{j_2} - (k - k_{j_2})\varpi$, where j_1 and j_2 denote the two planets and k, k_{j_2} are integers (in the present case, $j_1 = 6$, $j_2 = 5$, $k = 5$, and $k_5 = 2$). Using the Hamiltonian formulation, we adopt the canonical variables

$$\begin{aligned} S_1 &= L + \frac{k}{k_{j_2} - k}P, \quad & \sigma_1 &= \lambda - \lambda_{j_1}, \\ S_2 &= P, & \sigma_2 &= \frac{k_{j_2}\lambda_{j_2} - k\lambda}{k_{j_2} - k} - \varpi, \end{aligned} \qquad (2)$$

where $L = \sqrt{a}$ and $P = L(1 - \sqrt{1 - e^2})$. The other two degrees of freedom related to λ_{j_1} and λ_{j_1} are not explicitly given here (see, e.g., Morbidelli 2002). The Hamiltonian function is then averaged over λ_{j_1} and λ_{j_2}. The resulting system has two degrees of freedom. Our approach does not involve any expansions of the

gravitational potential of the planets. To evaluate the potential, we use the nonsingular algorithms of Moons (1993) for the 2 : 5 MMR with Jupiter and Nesvorný *et al.* (2002) for the coorbital motion. Consequently, the results are valid for high eccentricities and/or planet-crossing orbits.

Figure 5 shows the surfaces of section for six values of the "bi-circular energy." These surfaces of section have been computed on the angle $k\sigma_1 - k_{j_1}(k_{j_2} - k)\sigma_2$, which circulates with time. To identify the different energy levels, we show in Figs. 5a–5c the minimum eccentricity at each level. The energy levels are U-shaped in the (a, e) plane, with the minimum eccentricity occurring near the resonant center. For energies larger than the one shown in Fig. 5c, the energy levels descend to $e = 0$ at the semimajor axis indicated in each panel (Figs. 5d–5f) and open

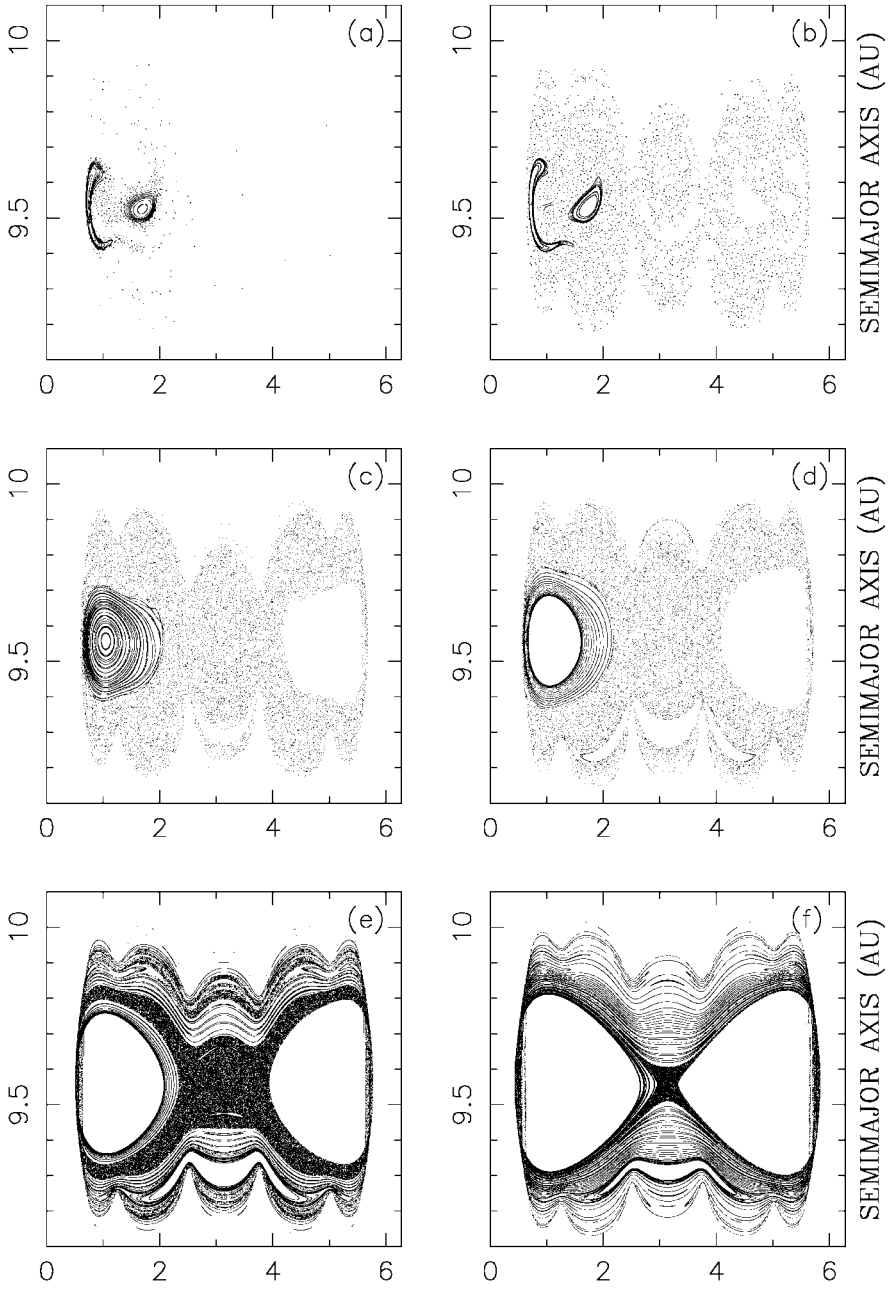

FIG. 5. The surfaces of section in the bi-circular model for Saturn Trojans. This two-degree-of-freedom model shows the interaction between the 1 : 1 MMR with Saturn and the 2 : 5 MMR with Jupiter. The overlap of these two resonances generates chaos for orbits close to the tadpole center and $e \gtrsim 0.13$ (a, b). Low-amplitude tadpole orbits are regular only at small eccentricities (c). These orbits are, however, driven to large eccentricities ($\gtrsim 0.13$) when secular dynamics is accounted for. (a) $e = 0.135$ at $a = 9.56$ AU; (b) $e = 0.12$ at $a = 9.56$ AU; (c) $e = 0.03$ at $a = 9.56$ AU; (d) $a = 9.43$ AU at $e = 0$; (e) $a = 9.36$ AU at $e = 0$; (f) $a = 9.31$ AU at $e = 0$.

at larger e. Thus, Figs. 5a–5f show the situation in the resonant region in a sequence of images, progressively going from higher (Fig. 5a) to lower e (Fig. 5c) at the resonant center, and to larger amplitudes (Figs. 5d–5f).

The surfaces of section demonstrate that the 2 : 5 MMR with Jupiter produces large-scale chaos in Saturn's coorbital space. This chaos may be understood in terms of the overlap criterion of Jupiter's 2 : 5 and Saturn's 1 : 1 MMRs (Chirikov 1979). Note that near the resonant center, regular trajectories exist only at small eccentricities (Fig. 5c). For $e > 0.12$, the niche of regular trajectories is very limited.

To understand the structure of the regular and chaotic orbits in the (a, e) plane in more detail, we performed several surveys of the dynamical stability in the frame of the bi-circular model. The test bodies were started with $\sigma_1 = \sigma_c(e)$ and $\sigma_2 = \pi$. Other choices of σ_2 do not change the results. The integration time span was 10^5 years. The test body was eliminated if it became a planet-crosser and was not phase protected from a collision.

In addition to Saturn's case, we ran the same survey in the bi-circular models for Jupiter's Trojans (accounting for the 5 : 2 MMR with Saturn) and for Uranus and Neptune. The latter two planets are close to a 2 : 1 MMR; the angle $\lambda_7 - 2\lambda_8$ circulates with a period $\approx$4230 years. Hence, for Uranus' Trojans, we account for the 2 : 1 MMR with Neptune $(\lambda - 2\lambda_8 + \varpi)$. For Neptune's Trojans, we account for the 1 : 2 MMR with Uranus $(2\lambda - \lambda_7 + \varpi)$. The results are shown in Fig. 6.

Jupiter's Trojans are practically unaffected by the 5 : 2 MMR with Saturn. The large stable region seen in Fig. 6a is much wider than the stable region shown by the numerical survey in Section 2 (Fig. 2a). Some mechanism other than the 5 : 2 MMR with Saturn must be responsible for this difference. The boundary between the regular and chaotic motions in the bi-circular model is sharp, and we checked that by integrating the bi-circular model over 10^6 years the result does not change.

As expected, an interesting case is that of Saturn's Trojans (Fig. 6b). Note the V-shaped unstable region near the tadpole

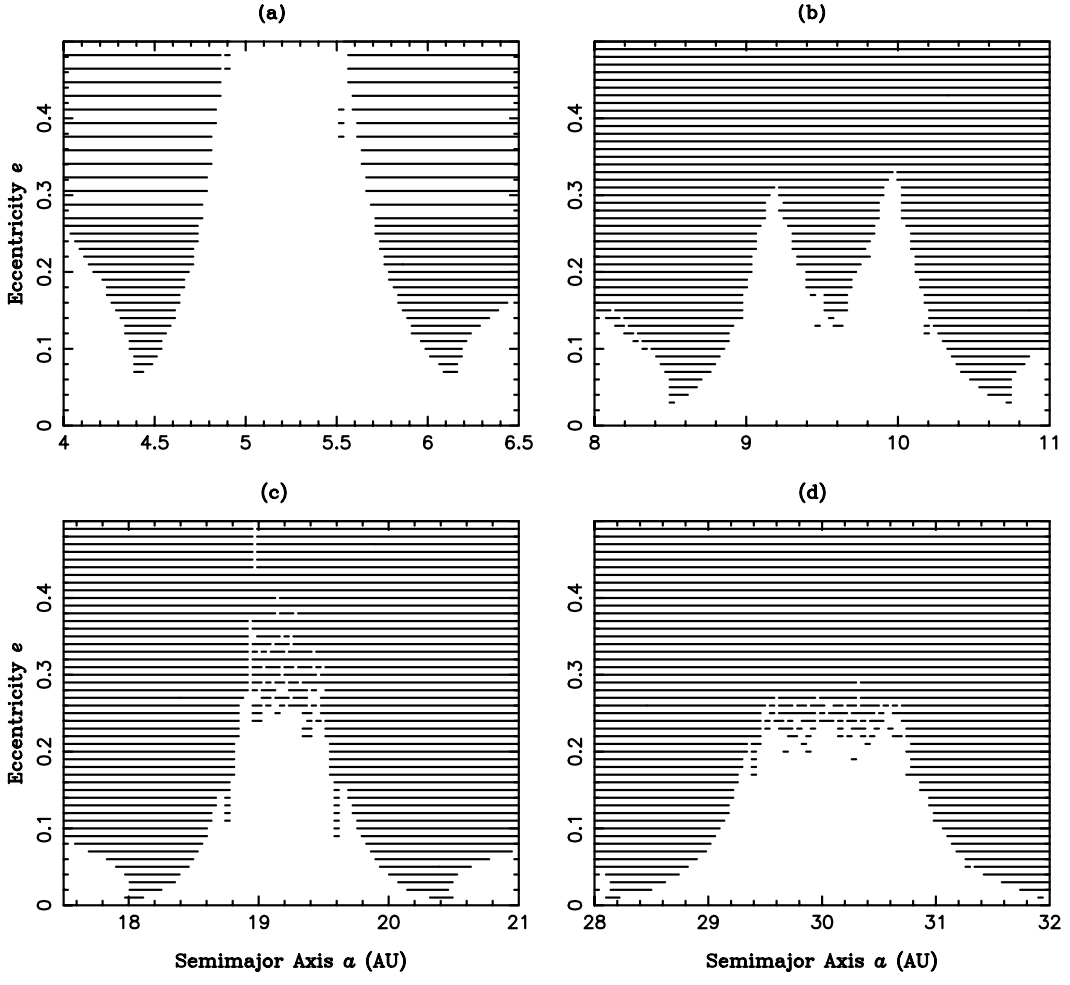

FIG. 6. The surveys of dynamical stability in the bi-circular model: (a) Jupiter, (b) Saturn, (c) Uranus, and (d) Neptune. Short horizontal line segments were plotted at the initial position of orbits which collided with a planet within 10^5 years. While Jupiter Trojans do not suffer from the Great-Inequality-generated instabilities (a), a V-shaped instability develops in Saturn's coorbital space due to the 2 : 5 Jupiter MMR (b). The eccentricities of Uranus' and Neptune's hypothetical Trojans must be limited to small eccentricities as a result of the instability which develops at $e \gtrsim 0.25$ and $e \gtrsim 0.2$, respectively, due to the near-commensurable orbital motion of these planets.

center at ≈9.6 AU. What happens there is that the 2 : 5 MMR with Jupiter, which grows in size with the eccentricity as $e^{3/2}$, is large at $e \gtrsim 0.13$ and its overlap with Saturn's 1 :1 MMR creates the chaotic domain (also seen in Figs. 5a and 5b). This observation is especially interesting in the context of the instability near the resonant center detected by more realistic surveys (e.g., Holman and Wisdom 1993 and our Fig. 2b).

We presume that the general instability near Saturn's Lagrangian points is due to the V-shaped instability in the bi-circular model seen in Fig. 6b and to the secular dynamics (Fig. 1b). Indeed, in the real situation (secular oscillations of e are absent in the bi-circular model), the eccentricities of most orbits near the resonant center undergo large secular oscillations with maximum values >0.1. For a trajectory near the resonant center ($a \sim 9.55$ AU), such an eccentricity is enough to switch on the fast instability originating from the overlap with the 2 : 5 Jupiter MMR (Fig. 6b), and a hypothetical saturnian Trojan moving on such a trajectory escapes. The same does not happen at tadpole orbits of larger amplitudes because, according to Fig. 6b, the eccentricity required to reach the strongly unstable region is larger ($e \gtrsim 0.2$).

Figure 1b suggests that there might exist a small region near $\varpi - \varpi_6 \sim 60°$ and $e \sim 0.07$ where e stays smaller than 0.1. The portrait of secular dynamics shown in this figure was, however, simplified by neglecting terms other than the first in the Fourier expansion of $e_6 \cos \varpi_6$. Accounting for other terms, the resulting secular evolution of e would be more complex. There are good reasons to believe that in the real case, the eccentricity of a small body is generally driven to values exceeding 0.1.

Consequently, we suggest that two mechanisms—secular oscillations of e and the Great-Inequality-generated chaos at $e > 0.1$—are involved in the origin of instabilities near the Lagrangian points of Saturn. Numerical simulations of the real problem (H. Scholl, personal communication) seem to confirm this hypothesis.

The reason why Jupiter's 2 : 5 MMR affects Saturn's Trojans so much while Saturn's 5 : 2 MMR has a negligible effect on Jupiter's Trojans (compare Figs. 6a and 6b) is mainly because of the mass difference between these planets, and also because MMRs exterior to a planet (such as Jupiter's 2 : 5) are generally wider than MMRs interior to its orbit (such as Saturn's 5 : 2). Consequently, Saturn's 5 : 2 MMR is very narrow and does not interfere much with the evolution of Jupiter's Trojans.

The orbits near the L_4 points of Uranus and Neptune are significantly affected by the quasi-resonant motion of these planets (Figs. 6c and 6d). The stable motion in the bi-circular model is limited to $e < 0.25$ for Uranus and $e < 0.2$ for Neptune. For Neptune, for which the forced secular oscillations of e are small (Fig. 1d), there must exist mechanisms other than the MMRs' overlap which limit the stable region in the realistic survey to $e \lesssim 0.08$ (Fig. 2d).

Michtchenko *et al.* (2001) attempted to constrain the primordial migration of the giant planets due to planetesimal scattering (Fernández and Ip 1984, Hahn and Malhotra 1999) and found that if Jupiter and Saturn had passed through the 2 : 1 or 5 : 2 resonance with each other, jovian Trojans would have been destabilized in $\lesssim$1 Myr. Beaugé *et al.* (2002) considered the effect of migration on the stability of orbits of the irregular satellites of the giant planets. Gomes (1998) suggested that planetary migration can explain: (i) the lack of Saturn's Trojans and (ii) the purported asymmetry in numbers of observed bodies in the L_4 and L_5 swarms of Jupiter. Gomes (1998) further argued that the Trojan populations become destabilized by MMRs which sweep through the coorbital space of planets. Since our bi-circular model is suitable for studying such effects of MMRs, we performed tests of Gomes's hypotheses using this approximation.

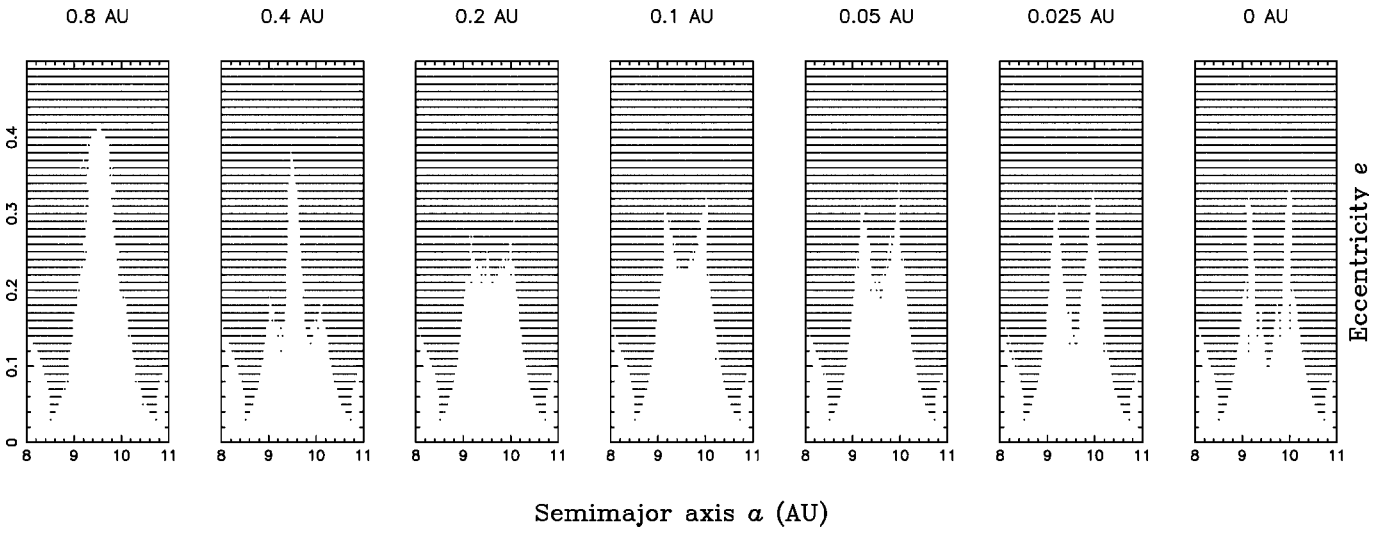

FIG. 7. The dynamical stability of orbits at Saturn's L_4 point during the planetary migration. The number above each graph indicates the distance of Saturn from the exact 2 : 5 MMR with Jupiter. Orbits unstable on 10^5-year time scales in the bi-circular model are shown by dots. See text for discussion.

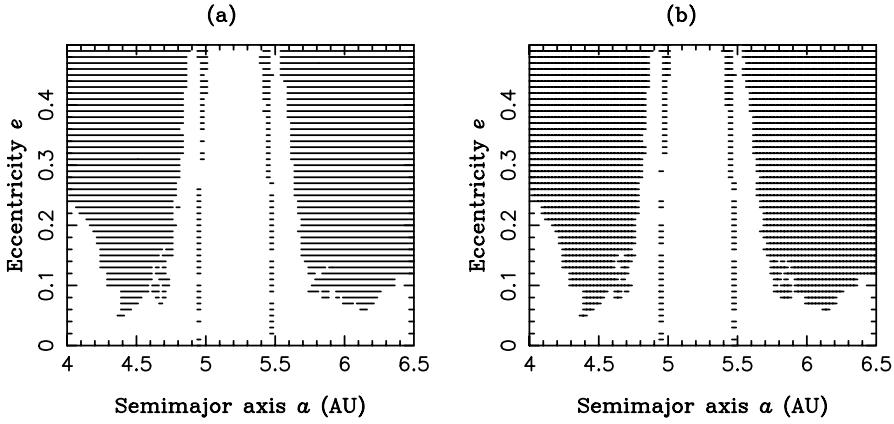

FIG. 8. The stability of Jupiter's (a) L_4 and (b) L_5 Trojans in a situation where Jupiter and Saturn are in the exact 2 : 1 MMR. Orbits unstable on 10^5-year time scales in the bi-circular model are shown by short horizontal line segments. No asymmetry between L_4 and L_5 orbits occurs. Similarly, no asymmetry occurs for the other, near-resonant locations of the planets, presumably taken at the beginning of the planetary migration. Consequently, the commensurable motion between the planets does not explain the unequal numbers of Jupiter's L_4 and L_5 Trojans that are observed.

In the first test, designed to verify (i), we mutually displaced Jupiter and Saturn to values presumably taken by Jupiter's and Saturn's semimajor axes at different epochs of their radial migration. We averaged out all terms in the Fourier expansion of Jupiter's gravitational potential except the terms responsible for the 2 : 5 MMR, and we treated the dynamical system in the frame of the bi-circular model. This treatment allowed us to isolate the effect of the 2 : 5 MMR with Jupiter on Saturn's coorbital bodies during the migration phase.

Figure 7 shows the result of our survey. We show snapshots of the orbital stability at different stages of the migration. The number above each graph indicates the distance of Saturn from the exact 2 : 5 MMR with Jupiter (Δ). This distance decreased during the migration to its present value of $\Delta \approx 0.025$ AU. Thus, Fig. 7 can be seen as a sequence of time steps from left to right. At the beginning of the "nominal" migration (Fernández and Ip 1984) when $\Delta \approx 0.8$ AU, most of the coorbital space of Saturn was stable according to Fig. 7. Note, however, that our model excludes resonances other than the 2 : 5 MMR with Jupiter, such as, e.g., the 1 : 2 MMR with Jupiter, which was quite important at the beginning of the migration. As soon as $\Delta \approx 0.4$ AU, the 2 : 5 MMR with Jupiter started to interfere with Saturn's Trojans, causing instabilities at $e \gtrsim 0.15$ for *moderate*-amplitude tadpole orbits. This instability region then progressively changed. For $\Delta \approx 0.025$ AU (today's value), most of the *small*-amplitude tadpole orbits with $e \gtrsim 0.13$ are unstable in the bi-circular problem. Since secular oscillations of e are expected to induce such eccentricities (Fig. 1b), we conclude that the radial migration of planets could have, indeed, caused a significant depletion of the preexisting population of Saturn's primordial Trojans at small to moderate libration amplitudes.

In the second test, designed to verify (ii), we displaced the semimajor axis of Saturn to induce an interference of its 2 : 1 MMR with Jupiter's L_4 and L_5 Trojans. Figure 8 shows the orbital stability of Jupiter's L_4 and L_5 Trojans. We note in this figure that no asymmetry between L_4 and L_5 occurs. Both Figs. 8a and 8b are characterized by equally large regions of stable motion. The vertical ridges of unstable motion at 4.95 and 5.48 AU are located at the separatrix between tadpole and horseshoe orbits (compare with Fig. 3a). The 2 : 1 MMR with Saturn apparently causes this structure by inducing chaotic motion near the separatrix. We thus conclude that the bi-circular problem gives us no hints about the possible asymmetry between the stability of Jupiter's L_4 and L_5 Trojans in early stages of planetary radial migration. Thus, the observation of Gomes (1998) that the L_5 Trojans are less stable due to Saturn's 2 : 1 MMR is not confirmed by our experiment. Jedicke *et al.* (2002) showed that the larger number of discovered jovian L_4 Trojans relative to L_5 Trojans probably resulted from observational biases.

4. FOUR-GYR, LOW-RESOLUTION SURVEYS

To access the dynamical stability of the outer planets' Trojans over the age of the Solar System, we numerically integrated 200–300 test bodies near the L_4 point of each planet over 4 Gyr. Since the stability of Jupiter's Trojans on gigayear time scales is known (Levison *et al.* 1997), we surveyed the Trojans of Saturn, Uranus, and Neptune. The goal of these integrations was to determine whether the hypothetical primordial Trojan populations of these planets could have survived until present times. We used the swift_rmvs3 symplectic integrator (Wisdom and Holman 1991, Levison and Duncan 1994) with a time step of 0.5 years.

To keep a one-to-one correspondence between this study and the high-resolution survey in Section 2, we use the same planets' positions and velocities and the same initial orbital angles of the test bodies. The semimajor axes and eccentricities of test bodies were chosen within the range of the small LCE in Figs. 2b–2d. We also sample several values of inclination: $i = 0°, 5°, 10°, 15°, 20°$ for Saturn and $i = 0°, 5°, 10°, 15°, 20°$, and $25°$ for Uranus and Neptune.

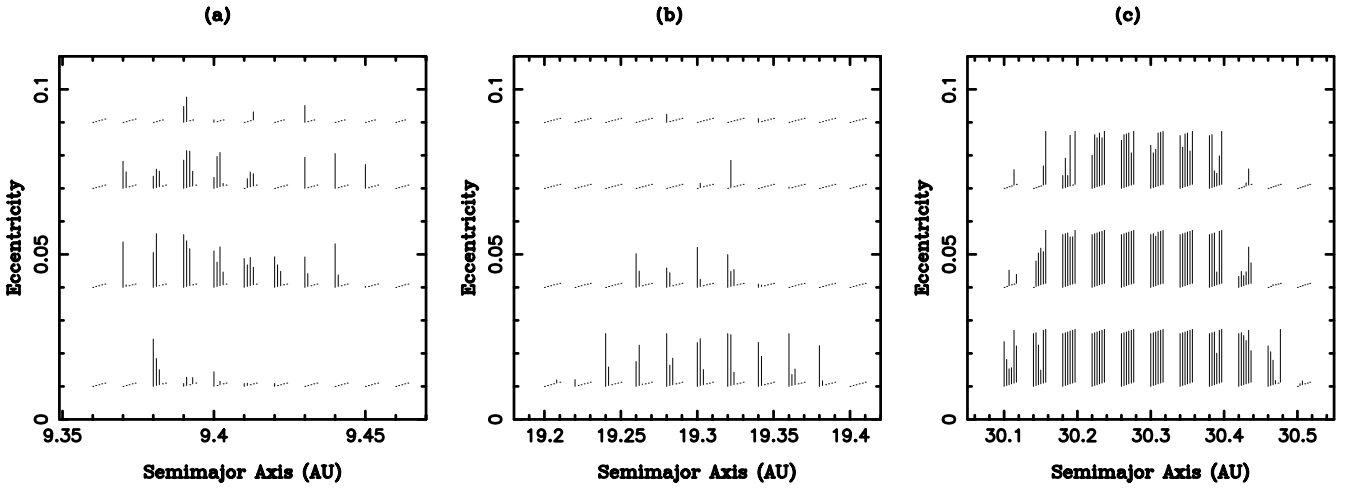

FIG. 9. Survival times of objects near Saturn's (a), Uranus' (b), and Neptune's L_4 (c) in our long-term surveys. The meaning of the bar code is explained in the text. Note the large island of stability at Neptune's L_4, contrasting with the general instability of tadpole orbits of Saturn and Uranus.

Figure 9 shows the orbital stability near each outer planet's L_4 point. The survival time ($t_{\rm surv}$) of each orbit is denoted in terms of a bar code: For Saturn (Fig. 9a), where there are five values of i per one initial (a, e), there are five line segments whose length is proportional to $\log_{10}(t_{\rm surv}) - 8$. Consequently, orbits with $t_{\rm surv} < 10^8$ years are denoted by a dot, while the longest line segments correspond to $t_{\rm surv} = 4 \times 10^9$ years. The leftmost line segment corresponds to $i = 0$, and the rightmost one corresponds to $i = 20°$. The same coding was used for Uranus and Neptune, except there are six line segments per one value of (a, e), the rightmost one corresponding to $i = 25°$.

Only two bodies from the initial 211, i.e., a fraction $f \approx 1\%$, survived over 4 Gyr on tadpole orbits with Saturn (Fig. 9a; see also Fig. 10, where the fraction of the surviving bodies versus time is shown). The most stable region is characterized by $a = 9.39$ AU, $e = 0.04$, and small i, which is well in the center of the bluish region in Fig. 2b of LCE $< 10^{-5.4}$ year^{-1}. Conversely, in the small-LCE region at $a = 9.44$ AU and $e = 0.05$ (Fig. 2b), no test body survived over 4 Gyr (Fig. 9a). There exists no direct one-to-one correspondence between our initial orbits and those used by Melita and Brunini (2001). Hence, the comparison of Fig. 9a with this previous work is not straightforward. Our results suggest that Saturn's Trojans are only marginally stable for libration amplitudes 50°–80°, $e < 0.1$, and small i. The population characterized by such orbits should have been reduced to $\approx$1% of the original number by instabilities acting over 4 Gyr.

Uranus' Trojans are also very unstable: Only four test bodies from the initial 264, i.e., $f \approx 1.5\%$, survived over 4 Gyr. The orbits of these stable bodies were initially placed close to Uranus' L_4 point and had $e \approx 0.01$ and $i < 5°$ (Fig. 9b). Unlike the case of Saturn's L_4 orbits, for which the escape rate was roughly constant with $\log_{10} t$ during the entire history of the Solar System (Fig. 10), Uranus' L_4 orbits evaporate relatively faster at $10^6 < t < 10^8$ years and more slowly at earlier and later times. This fact probably relates to different dynamical mechanisms destabilizing the populations.

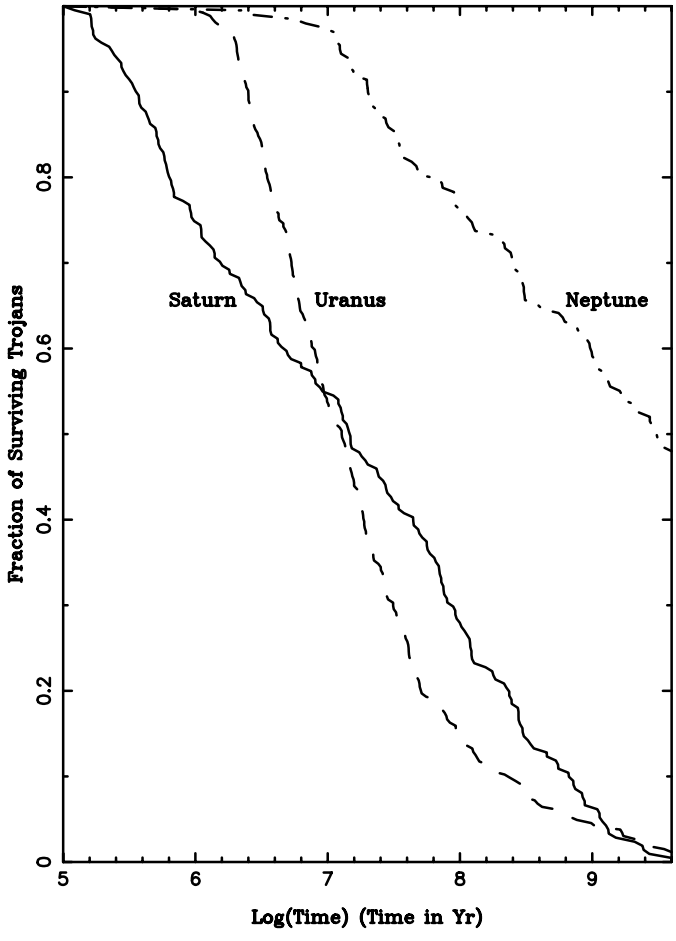

FIG. 10. Fraction of surviving test bodies at tadpole orbits with the outer planets. The test bodies were initially placed near the L_4 points of the outer planets according to the recipe described in the text. The endpoint on the x axis corresponds to 4 Gyr. While Saturn's and Uranus' Trojans were depleted by a factor of $\approx$100, about 50% of test bodies survive over 4 Gyr on Neptune's tadpole orbits.

Our results suggest that the hypothetical primordial Trojan populations of Saturn and Uranus have been drastically reduced by dynamical instabilities acting over the ~4-Gyr age of these planets. If such populations were initially characterized by densities resembling the present Trojans of Jupiter, we estimate that not more than a few tens of saturnian and uranian Trojans with 10 km and larger radii can currently exist (see Sections 5 and 6). Such small populations would not have been detected by previous observational searches. It is nevertheless likely that processes like the radial migration of planets (Fernández and Ip 1984) and the excitation of e and i of small bodies during their accretion (Petit *et al.* 1999) should have severely depleted these populations in addition to the long-term dynamical instabilities. Thus, we argue that the existence of large population of saturnian or uranian Trojans of 10-km radii is rather unlikely.

The case of Neptune's L_4 point is very different (Fig. 9c and Fig. 10). Forty-eight of 100, or $f = 48\%$ of our test particles, survived for 4 Gyr. The region around L_4 is characterized by a large stability region of some 0.4 AU width and eccentricities up to 0.08. What is even more striking is the extent of the stable region in inclination. We ran the orbits up to $i = 25°$ in our survey, not expecting, from the experience with Saturn and Uranus, to detect any such highly inclined stable objects. The opposite proved to be true: There are cases at $e = 0.07$ (Fig. 7c) where more inclined orbits survive, while those with $i \sim 0°$ do not (note, for instance, the orbits starting at $a = 30.3$ AU and $e = 0.07$). We show later that the stability region extends to $i \approx 35°$ (Section 5, Fig. 12).

The extent of the stable region at Neptune's L_4 may also by quantified in terms of the libration amplitude of $\lambda - \lambda_8$. Most orbits with initial amplitudes $<60°$–$70°$ at small e last for 4 Gyr. A similar result has been obtained by Weissman and Levison (1997), who found that Neptune's Trojans started with small proper eccentricities are generally stable unless libration amplitudes initially exceeded $\approx 60°$. Although we did not study Neptune's L_5 orbits in similar detail, there is good reason to believe that an equally large and robust stability region also exists there.

The region near Neptune's L_4 and L_5 points that is stable over the age of the Solar System is significantly larger and more robust than the one found by Holman (1997) between Uranus and Neptune. While the majority of Neptune's Trojans with $e \lesssim 0.08$ and $i \lesssim 35°$ survive over 4 Gyr, the belt suggested by Holman (1997) is marginally stable at $e \lesssim 0.01$ and $i \lesssim 1°$ for 1 Gyr, Neptune's Trojans are also much less sensitive to other primordial processes that could have erased the hypothetical belt between Uranus and Neptune (Brunini and Melita 1998). Nevertheless, a large primordial migration of Neptune could have increased the resonant amplitudes of its Trojans by several tens of degrees, in analogy to the response of jovian Trojans to a slowly evolving planetary semimajor axis (Fleming and Hamilton 2000). Such evolution could have partially eroded the preexisting population.

Another important subject concerns the origin of Neptune's Trojans. It was shown that in the case of Jupiter's Trojan swarm, the important mechanism of capture could have been the fast contraction of the gaseous envelope onto the planet. Jupiter gained most of its mass during this gas-accretion phase (Pollack *et al.* 1996). As a consequence of the planet's growth, the space available to the coorbital bodies was substantially enlarged. Calculations showed that such a process could have been nearly 50% effective in capturing bodies on tadpole orbits (Marzari and Scholl 1998).

It is likely that Neptune accreted the bulk of its mass during an interval of 10^7 years or longer (Bryden *et al.* 2000, Levison and Stewart 2001), which was probably orders of magnitude longer than the time scale of the contraction of Jupiter's gas envelope (Pollack *et al.* 1996). Hence, the efficiency of captures onto tadpole orbits was probably lower in the case of Neptune because many bodies were scattered by or collided with Neptune before reaching Trojan-like orbits. Nevertheless, if Neptune did not undergo a very violent stage of orbital changes (as for instance the one suggested by Thommes *et al.* 1999, 2002), a significant primordial population of Neptune's Trojans could have been formed.

We thus conjecture that coorbital regions near Neptune's L_4 and L_5 points may host an important population of primordial bodies. Such a population would have been reduced only by a factor ≈ 2 (from our set of orbits, $\approx 50\%$ of bodies survive over 4 Gyr; Fig. 10) due to dynamical instabilities and may constitute a yet to be discovered component of the inventory of the Solar System.

5. THE APPEARANCE OF HYPOTHETICAL TROJAN POPULATIONS ON THE SKY

Results of our long-term surveys can be used to compute the expected sky densities of hypothetical Trojan populations of the outer planets. We investigated three cases: (1) The Model I population was derived from the surveys described in Section 4, where the initial i, e, and A_σ of tadpole orbits were *uniformly* sampled; (2) The Model II population was derived assuming that the Trojans' formation mechanism *randomly* sampled heliocentric orbits; and (3) Model III assumes that the Trojans of each giant planet follow Rayleigh distributions in i and e with mean values similar to those of Jupiter's Trojans. Models I and II differ since the physical volume available to tadpole orbits is a function of their i, e, and A_σ. For example, the initial inclination distribution of Model II is $f(i)\,di = \sin i\,di$ (Section 6.2), unlike the uniform i distribution in Model I.

Models I and II should roughly cover the range of possible orbital distributions of Trojans. Model I can be seen as a limiting case, which must be convolved with the primordial orbital distribution of Trojans to derive a realistic result. We made this choice, since the capture/formation process of Trojans is to a large degree unknown except for Jupiter, where the suspected mechanism is the fast increase of the planet's mass by the contraction

of the gas envelope (Marzari and Scholl 1998). Moreover, we further assumed that no subsequent excitation of i, e, and A_σ occurred. This apparently is inconsistent with the current orbital distribution of Jupiter's Trojans, which have rather large i, e, and A_σ (see, e.g., Yoder 1979, Marzari and Scholl 2000, and Marzari *et al.* 2002). We wish to make clear that the Model I population should be seen just as a reference case for the effect of the long-term dynamical erosion, and not as an attempt to realistically reproduce the unknown distribution of Saturn's, Uranus', and Neptune's Trojans. Conversely, Model II attempts to reproduce these populations using several assumptions and is probably a more realistic basis for guiding observational searches (see Section 5.2).

5.1. Model I

We use the results of the simulations described in Section 4. For Neptune, we account only for bodies which survived 4 Gyr and make use of their evolution in the last 10^8 years of the simulation (i.e., between 3.9 and 4 Gyr). The orbital element distribution of these bodies is nearly stationary in the last gigayear. Moreover, the 10^8-year interval is long enough to sample all phases of the secular angles. This selection represents our Model I population of the hypothetical present-day Trojan swarm at the L_4 point of Neptune.

At each time output (i.e., every 10^4 years), positions and velocities of the model bodies were referred to the instantaneous orbital plane of Neptune and its instantaneous position. The longitude ($\Delta\theta$) and latitude ($\Delta\phi$) were computed in the same reference system. Referring $\Delta\theta$ and $\Delta\phi$ to the planet's instantaneous orbital plane is a good choice, because the Trojan's motion is symmetric with respect to this plane (and not the ecliptic, for instance).

We then divided the sky into $1^\circ \times 1^\circ$ segments and computed the total residence time spent by bodies of the model population within each segment. In a steady state, the total residence time is proportional to the number of objects residing in each segment at any time. Under this assumption, the resulting plot represents the expected sky density of Neptune's Trojans. Moreover, we normalized the sky density $\rho_{\rm sky}$ by assuming the total number of hypothetical Trojans residing near the L_4 point of the planet to be equal to 1. For this reason, the plots represent the probability of finding an object in a segment.

For Saturn and Uranus, where only two and four bodies, respectively, survived over 4 Gyr (so that our statistics were poor), we performed the same procedure but accounted only for bodies surviving at 1 Gyr using their orbital history from 0.9 to 1 Gyr. Such model populations of saturnian and uranian Trojans consisted of 14 and 12 bodies, respectively. The derived sky density distributions from these model populations are expected to be somewhat broader than those surviving 4 Gyr.

Figure 11 shows the normalized sky densities (probabilities) for the outer planets' L_4 Trojans, as viewed from the Sun. Saturn's case is peculiar because of the instability near L_4. The largest densities occur near longitudes that differ from Saturn's

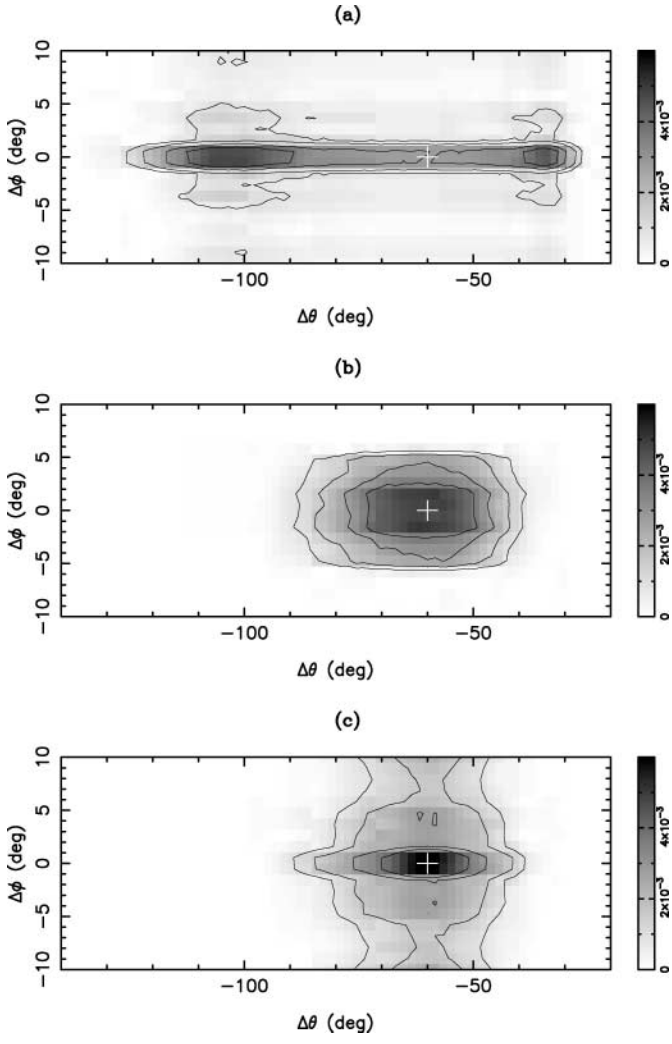

FIG. 11. The normalized sky densities $\rho_{\rm sky}$ of Model I Trojans at the L_4 points of Saturn (a), Uranus (b), and Neptune (c). The contour lines correspond to $\rho_{\rm sky} = 0.003$, 0.002, 0.001, and 0.0005 deg^{-2}. In the case of Saturn, the largest densities appear displaced from the position of the L_4 point (white cross) since low-amplitude tadpole orbits are unstable. For Uranus and Neptune, the largest densities occur near the L_4 point.

by $\Delta\theta = -105^\circ$ and -35°, where $\rho_{\rm sky} = 0.003$–0.004 deg^{-2}. The high densities are localized within a few degrees of the planet's orbital plane. As Saturn's inclination with respect to the ecliptic is currently about 2.5°, the high-density segments may be offset from the ecliptic by as much as this amount, depending on the time of observation.

Uranus' hypothetical L_4-Trojan population is concentrated near $\Delta\theta = -60^\circ$ (Fig. 11b). The 0.003 contour plot (the innermost one) comprises some 100 deg^2. This is a large area; for comparison, Uranus' Hill sphere corresponds to only $\approx$7 deg^2. Any observational survey with a reasonable chance to discover hypothetical Trojans of Uranus must thus cover an equivalent of many Hill spheres near the L_4 point. This is obviously a much harder, and likely to be less rewarding, task than that which

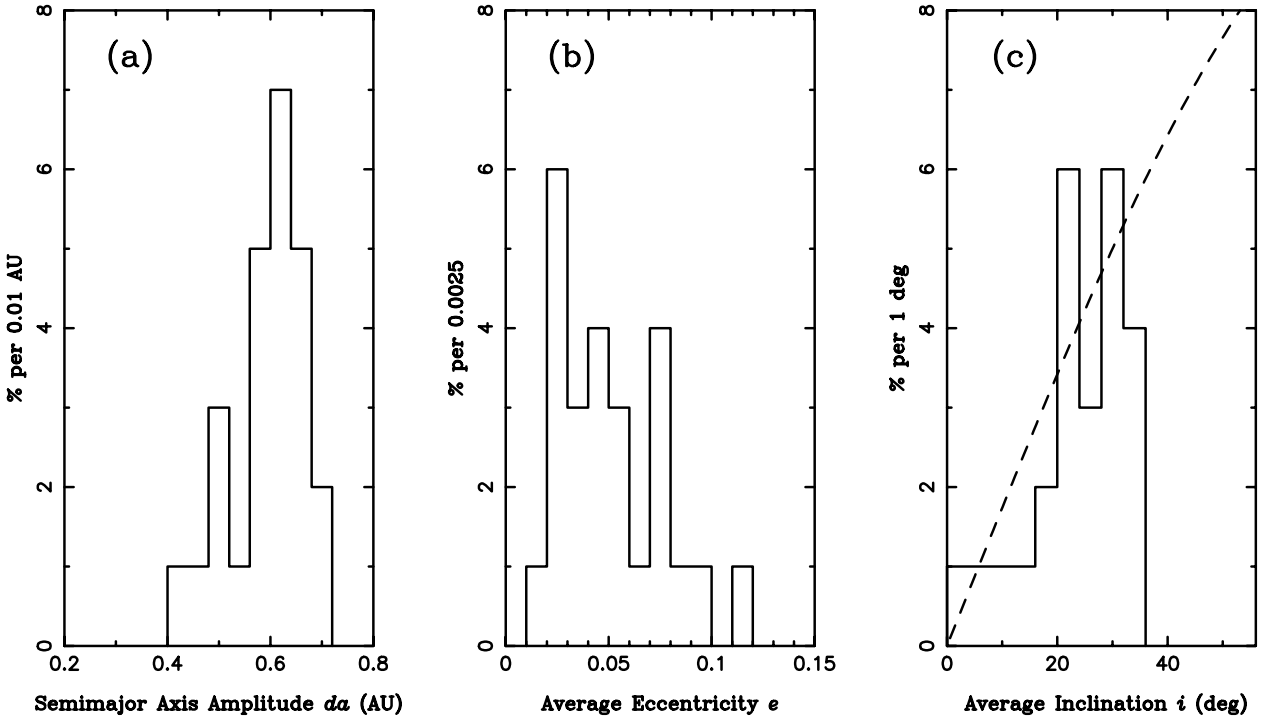

FIG. 12. The orbital distribution of the surviving population of Model II Neptune Trojans. Orbital elements determined from a 3.99- to 4.00-Gyr interval are shown: (a) semimajor axis amplitude, (b) averaged eccentricity, and (c) averaged inclination.

resulted in recent discoveries of Uranus' irregular satellites (Gladman *et al.* 1998a).

The sky density plot for Neptune is probably the most interesting one because our long-term survey showed that nearly 50% of primordial neptunian Trojans survive 4 Gyr. In this case, the high densities appear to be tightly clustered near the L_4 point (Fig. 11c). The $\approx$10 deg^2 area centered at the L_4 point would be a good target for devoted observational surveys. This area contains some 2% of our Model I population of Neptune's L_4 Trojans. We will, however, see in the next section that the tight clustering of Model I bodies around the L_4 point is, to a large degree, due to the assumption of the initially uniform i, e, and A_σ. When convolved with a realistic starting population (Section 6.2), Neptune's Trojans become much more dispersed, showing large sky densities in extended regions around the L_4 and L_5 points.

A ground-based-telescope search for an outer planet's Trojans will see the largest densities somewhat displaced in $\Delta\theta$, depending on the position of the Earth at the time of observation. If the observation is performed when the L_4 point is at opposition, these displacements are about $-5°$, $-2.5°$, and $-1.7°$ for Saturn, Uranus, and Neptune, respectively. Negative values mean that the high-density segments occur at larger longitudinal distances from the planet than in Fig. 11.

We focused our analysis on the L_4 points of the outer planets. We have, however, also performed a brief analysis of the L_5 points. This analysis did not reveal any substantial difference in stability and dynamics between the leading and trailing Lagrangian points. Consequently, the sky densities at the L_5 points, trailing the planets' motion, should be mirror images (with respect to $\Delta\theta = 0°$) of the sky densities shown in Fig. 11.

5.2. Model II

We concentrate on Neptune's case here. The initial orbits for the Model II population were chosen according to a $1/a$ surface density distribution[1] in the range $29 < a < 31$ AU. We chose the inclination distribution $f(i)\,di = \sin i\,di$, which is the expected inclination distribution if L_z/L were uniformly sampled, where L and L_z are the heliocentric angular momentum and its z component, respectively. Eccentricities and orbital angles were chosen randomly in the ranges (0, 0.13) and (0, 360°), respectively. A total of 10,000 test bodies were numerically integrated for up to 4 Gyr or until they met their end.

From 27 bodies surviving over 4 Gyr, 25 bodies move on tadpole orbits at the end of the integration. The remaining two bodies move on Neptune-crossing orbits with large semimajor axes. In the following, we will only utilize the 25 bodies surviving on tadpole orbits. Figure 12 shows the distribution of their

[1] The results depend very weakly on the radial surface density profile, because the surviving populations, which are used to calculate the sky densities, have very limited radial extents (fractions of an astronomical unit).

orbital elements. In Fig. 12a, we plot the amplitude of the semimajor axis variations for each body determined as a difference between its maximum and minimum semimajor axis in the last 10-Myr interval (i.e., between 3.99 and 4 Gyr). Since perturbations by Jupiter cause ≈0.4 AU short-period variations of the semimajor axis of Neptune's Trojans, the amplitude shown in Fig. 12a is never less than 0.4 AU. The effect of these short-period variations could be seen in the surveys of Holman and Wisdom (1993), who found that the stable region associated with Neptune's L_5 point occurs at larger heliocentric a than that at the L_4 point. We argue that this asymmetry should not be viewed as a signature of asymmetric long-term instabilities acting at Neptune's L_4 and L_5 points but rather as originating from the choice of initial orbits.[2]

Figures 12b and 12c show the eccentricities and inclinations of 25 surviving Trojans averaged over the last 10 Myr of our integration. These figures reflect our choice of the initial distribution of stable orbits and the long-term erosion of the unstable orbits. In Fig. 12b, the forced eccentricity does not permit any orbits with averaged e smaller than 0.01. The part of the population at large e was significantly eroded, leaving only one body with $e > 0.1$. The dashed line in Fig. 12c shows the initial $\sin i$ distribution. The part of the population at $i \gtrsim 40°$ was removed by long-term instabilities.

We performed a similar experiment for Uranus's Trojans, integrating 10,000 bodies initially at $18 < a < 20$ AU. In this integration, all test bodies turned out to be unstable. The most long-lived body escaped at 185 Myr. This integration thus confirmed the much greater stability of Trojans of Neptune than those of Uranus.

Figure 13 shows the sky density of our Model II population of neptunian Trojans. This figure has been computed by the method described in Section 5.1. Note that the sky density in Fig. 13 is a much flatter function of sky coordinates (especially of $\Delta\phi$) than in Fig. 11c. This reflects the different initial orbital distributions of the Model I and Model II populations. Since the Model II population is expected to better resemble the orbital distribution of hypothetical neptunian Trojans, Fig. 13 is probably a better estimate of where these bodies appear on the sky. These are, however, bad news for observers, since in Fig. 13 no region shows a density larger than 0.0005 deg^{-2}. Thus, unless the population of Neptune's Trojans is very large, a large area on the sky should be searched to have a reasonable chance of success.

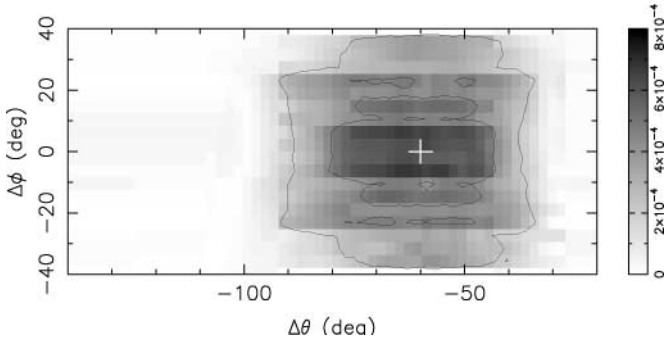

FIG. 13. The normalized sky density $\rho_{\rm sky}$ of Model II Trojans at the L_4 point of Neptune. The contour lines correspond to $\rho_{\rm sky} = 0.0003$ and 0.0001 deg^{-2}. Neptune's Trojans appear largely dispersed on the sky around the L_4 point. The flat latitudinal distribution is dictated by large inclinations of the surviving bodies (Fig. 12c).

A good strategy would probably be to utilize the current surveys of the Kuiper Belt and target most of the imaging within ±15° in longitude and ±10° in latitude of Neptune's Lagrangian points. This area contains some 25% of our Model II population. The motion of the planet's Trojans on the sky as viewed from the Sun very much resembles the motion of the planet itself. There should be, however, a significant component of the latitudinal velocity for highly inclined orbits.

5.3. Model III

In our final attempt to produce a "realistic" sky density distribution of the hypothetical Trojans of Neptune, we assume that their primordial eccentricities and inclinations obeyed Rayleigh distributions (Ida and Makino 1992). This assumption is motivated by the possible outcome of accretion at ∼30 AU. For the average values of eccentricities and inclinations we take $\langle e \rangle = 0.08$ and $\langle i \rangle = 13.7°$. These average values correspond to the current $\langle e \rangle$ and $\langle i \rangle$ of Jupiter's Trojans (Jewitt *et al.* 2000). We are not suggesting that these distributions of e and i necessarily apply to Neptune; clearly, the formation of Neptune's Trojans could have been much different from that of Jupiter's Trojans. Nevertheless, we use this assumption to check whether under these circumstances the Trojans of Neptune would appear more concentrated on the sky than in Fig. 13.

Figure 14 shows the sky density of Neptune's Trojans in this new model. As expected, the higher sky densities are now more concentrated toward the planetary plane than in Fig. 13. The central area within ±15° in longitude and ±10° in latitude of Neptune's Lagrangian points now contains some 75% of the surviving model population. In this area, the average sky density is about 0.001 deg^{-2}. The observational survey in this scenario may thus be 2 to 3 times more efficient than if Model II applies (Fig. 13). Nevertheless, large sky areas must still be covered. If the Rayleigh distributions of i with smaller $\langle i \rangle$ are used, the bins with high sky densities become more clustered around $\Delta\phi = 0$.

[2] The short-period oscillations of the osculating semimajor axis mainly occur due to the Sun's motion around the center of mass of the Sun–Jupiter system. The full amplitude of these oscillations is $\Delta a = \frac{2}{\pi} a^{3/2} \Delta v$, where $\Delta v \sim$ 0.003 AU/year is the Sun's velocity around the center of mass. Depending on the initial phase of a test body with respect to the line connecting Jupiter and the Sun, the initial heliocentric semimajor axis of the test body can be smaller or larger than its average over one Jupiter revolution around the Sun. This causes the appearance of the asymmetry of the L_4 and L_5 points observed by Holman and Wisdom (1993). Note that $\Delta a \propto a^{3/2}$, which means that more distant orbits suffer larger short-period oscillations. Indeed, the asymmetry between the L_4 and L_5 points observed by Holman and Wisdom (1993) is the largest for the Neptune Trojans.

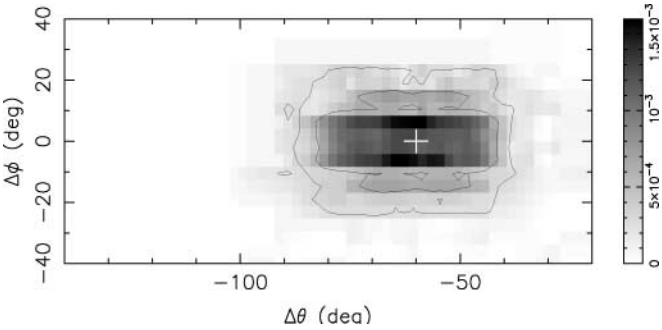

FIG. 14. The normalized sky density $\rho_{\rm sky}$ of Trojans at the L_4 point of Neptune. The eccentricities and inclinations of the primordial population were assumed to follow the Rayleigh distribution with $\langle e\rangle = 0.08$ and $\langle i\rangle = 13.7°$. The primordial population was dynamically evolved over 4 Gyr and projected on the sky. The contour lines correspond to $\rho_{\rm sky} = 0.0003$ and 0.0001 deg^{-2}. Also in this case, Neptune's Trojans appear widely dispersed on the sky around the L_4 point.

Such flat distributions are, however, unlikely since most of the small-body reservoirs in the Solar System have rather large i. The sky density distribution is not very sensitive to the assumed value of $\langle e\rangle$.

6. CONSTRAINTS ON PRESENT-DAY TROJAN POPULATIONS

We have crudely estimated the number of Trojans as a function of limiting magnitude that one might find at present at each of the giant planets. In the absence of a realistic calculation for the primordial number of Trojans for each planet, we assume that Saturn, Uranus, and Neptune *initially* had as many Trojans as Jupiter does *at present* and then calculate how many Trojans of a given magnitude (a) should exist in total at Saturn, Uranus, and Neptune, given the survival fractions we found previously, and (b) should have been discovered by observational surveys to date. Of course, this is only an order-of-magnitude estimate.

Jewitt *et al.* (2000) surveyed 20 deg^2 near Jupiter's L_4 point to a limiting magnitude $V \sim 22.5$ and found 93 Trojans. For Jupiter Trojans at opposition at heliocentric distance (5.1 AU), and assuming a geometric albedo 0.04, $r = 10^{0.2(24.23-V)}$, where r is the Trojan's radius in kilometers. For example, $V = 19.23$ corresponds to $r = 10$ km. Combining their results with those of previous surveys, Jewitt *et al.* find a broken, power law for the total number of Jupiter L_4 Trojans larger than radius r as $N(r) = 1.6 \times 10^5\, r^{-(2.0\pm0.3)}$, where r is measured in kilometers, for $2.2 \le r \le 20$ km and $N(r) = 7.8 \times 10^8\, r^{-(4.5\pm0.9)}$ for $r \ge 42$ km. This implies of order one 100-km Trojan at Jupiter; in fact, one, (624) Hektor, is known (Storrs *et al.* 1999). If we assume equal numbers of objects at the L_4 and L_5 points, these equations must be multiplied by a factor of 2 to get the total number of jovian Trojans.

If they have the same albedo as jovian Trojans, hypothetical Trojans of Saturn, Uranus, and Neptune will be fainter than jovian Trojans by approximately $dm = 5\log_{10}[a(a-1)/(5.1)(5.1-1)]$ magnitudes. Taking $a = 9.5$, 19.2, and 30.1 AU for these three planets, we have $dm = 2.93$, 6.12, and 8.11 mag, so that 10-km-radius Trojans of Saturn, Uranus, and Neptune should have $V = 22.2$, 25.3, and 27.3 mag (cf. Gladman *et al.* 1998b, 2000, 2001, Holman *et al.* 2001). Table I shows the number of jovian Trojans with radii larger than various values between 5 and 110 km and the V magnitude of such objects at opposition at each of the giant planets. Figure 15 shows the number of Trojans brighter than a given V magnitude that each planet would have if all four giant planets had as many Trojans as Jupiter (and identical size distributions).

Now, accounting for the survival fractions determined by our surveys (about 1% for Saturn and Uranus and 50% for Neptune), the most promising targets for observational surveys are Saturn and, especially, Neptune. Saturnian Trojans, being closer to the Sun, are about 3 magnitudes brighter than uranian Trojans. Neptunian Trojans have ≈50 times higher survival rates than uranian Trojans, which compensates for their being about 2 magnitudes fainter. There are, however, many unknowns involved in these estimates since, for example: (1) Saturn's Trojans could have been very susceptible to planetary migration; (2) the capture/formation mechanism of Trojans of the outer planets could have been different at different planets; and (3) the size distribution of jovian Trojans may not be representative for other planets' Trojans.

D. C. Jewitt (personal communication; see also Chen *et al.* 1997) surveyed about $A = 30$ deg^2 to V magnitude 22 and 0.7 deg^2 to V magnitude 25, generally near the triangular Lagrange points, to search for Trojans of Saturn, Uranus, and Neptune, and found none. Assuming average normalized sky densities of $\Sigma \approx 0.002$ (Fig. 11) and $\Sigma \approx 0.0005$ (Fig. 13) objects per deg^2 for Saturn and Neptune, respectively, the number of Trojans that should have been discovered is $N(V) f \Sigma A$. This corresponds to 1.6 and 0.6 saturnian Trojans at $V = 22$ and

TABLE I

The Total Population of Jovian Trojans, According to the Size Distribution of Jewitt *et al.* (2000), and Assuming Equal Numbers at L_4 and L_5

		V magnitude at opposition			
r (km)	$N(>r)$	Jupiter	Saturn	Uranus	Neptune
5	12,800	20.7	23.7	26.9	28.8
10	3200	19.2	22.2	25.3	27.3
20	800	17.7	20.7	23.8	25.8
42	77	16.1	19.0	22.2	24.2
50	35	15.7	18.7	21.9	23.8
100	2	14.2	17.2	20.3	22.3
110	1	14.0	17.0	20.1	22.1

Note. The columns show radius (r), the estimated number of Trojans larger than this radius ($N(>r)$), and the approximate V magnitude at opposition that Trojans of a given size would have at each of the giant planets, assuming a geometric albedo of 0.04.

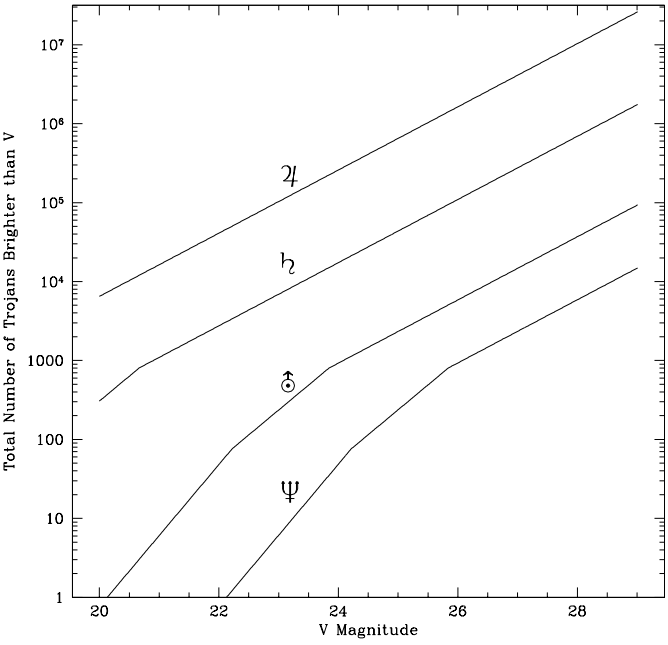

FIG. 15. The number of Trojans ($N(V)$) brighter than magnitude V that each of the giant planets would have, if they had the same population as Jupiter. We have adopted the size distribution for jovian L_4 Trojans of Jewitt *et al.* (2000). For radii between 20 and 42 km, we use the expression $N(r) = 1.0 \times 10^7 r^{-3.15}$ to interpolate between the two power laws given by Jewitt *et al.* Because of the broken-power-law size distribution we assume, the plot shows kinks at $V = 20.7$ for Saturn, $V = 22.2$ and 23.8 for Uranus, and $V = 24.2$ and 25.8 for Neptune.

$V = 25$, respectively, and 0.005 and 0.04 neptunian Trojans, respectively. Note that, if neptunian Trojans have the same size distribution as jovian Trojans, the size distribution is steep at V magnitudes less than 25.8, so the deeper survey provides a stronger constraint.

The upper limits provided by current observations are a saturnian population of order 1% of Jupiter's, consistent with our dynamical erosion estimates, and a neptunian population that could equal, or even vastly exceed, Jupiter's. Even if Neptune has 6000 Trojans with $V < 25$ ($r > 29.4$ km for an albedo of 0.04), a population 25 times that of Jupiter at the same size, Jewitt's survey would only be expected to discover one neptunian Trojan. A search near Neptune's L_4 or L_5 point of 10 deg^2 to $V = 26$ (R magnitude 25.5, assuming $V - R = 0.5$), would be expected to discover two Trojans if Neptune's primordial population equaled Jupiter's present population. The required search area is about 20 times larger than that searched in a Kuiper Belt survey to $R = 25.6$ carried out at Palomar in 1997, using a 2048^2 CCD (Gladman *et al.* 1998b, 2001), and about 7 times larger than the area searched in 1998 and 1999 with a mosaic of four 2048^2 CCDs at CTIO (Allen *et al.* 2001). Since much larger mosaic CCD cameras are now available (Trujillo *et al.* 2001), a deep search of 10 deg^2 appears feasible in the near future.

We estimate that $\lesssim$6000 neptunian Trojans should exist with $V < 25.0$. This constraint is about three times tighter than that of Weissman and Levison (1997), who estimated less than 500 $i_{\max}$ neptunian Trojans with $V < 25.0$, where $i_{\max}$ is the maximum inclination of neptunian Trojans. From Fig. 12c, we find $i_{\max} \sim 35°$, so Weissman and Levison's constraint implies that there are less than 17,500 neptunian Trojans with $V < 25$.

7. CONCLUSIONS

We summarize our main results as follows:

While Saturn's and Uranus' primordial populations of Trojans should have been reduced by a factor of $\approx$100 by dynamical instabilities acting over 4 Gyr, Neptune's Trojans are significantly more stable. This suggests that a substantial population of neptunian Trojans may exist.

If Neptune's Trojans do exist, they may be dispersed widely on the sky because even orbits with inclinations $\sim$30° near Neptune's Lagrangian points are generally stable. A population of neptunian Trojans larger than Jupiter's cannot be ruled out by observational searches to date.

The origin of the strong instability at Saturn's Lagrangian points probably results from the secular dynamics which raises small-body eccentricities to $\gtrsim$0.13, where strong chaos exists due to the overlap with the 2 : 5 MMR with Jupiter.

The marginally unstable region at Jupiter's Lagrangian points where the lifetimes range between 10^7 and 10^9 years is suggested to be related to three-body resonances. A similar situation occurs in other MMRs in the asteroid and Kuiper belts.

ACKNOWLEDGMENTS

We thank David Jewitt and Hans Scholl for providing results in advance of publication; Brett Gladman, Doug Hamilton, Hal Levison, Francesco Marzari, and Alessandro Morbidelli for interesting discussions; and Hans Scholl and an anonymous referee for their reviews.

REFERENCES

Allen, R. L., G. M. Bernstein, and R. Malhotra 2001. The edge of the Solar System. *Astrophys. J.* **549**, L241–244.

Beaugé, C., F. Roig, and D. Nesvorný 2002. Effects of the planetary migration on natural satellites of the outer planets. *Icarus* **158**, 483–498.

Benettin, G., L. Galgani, and J. M. Strelcyn 1976. Kolmogorov entropy and numerical experiments. *Phys. Rev. A* **14**, 2338–2345.

Bretagnon, P., and J.-L. Simon 1990. General theory of the Jupiter–Saturn pair using an iterative method. *Astron. Astrophys.* **239**, 387–398.

Brunini, A., and M. D. Melita 1998. On the existence of a primordial cometary belt between Uranus and Neptune. *Icarus* **135**, 408–414.

Bryden, G., D. N. C. Lin, and S. Ida 2000. Protoplanetary Formation. I. Neptune. *Astron. J.* **544**, 481–495.

Chen, J., D. Jewitt, C. Trujillo, and J. Luu 1997. Mauna Kea Trojan Survey and Statistical Studies of L_4 Trojans. *Bull. Am. Astron. Soc., 1020* **29**, [abstract #25.08.]

Chirikov, B. V. 1979. A universal instability of many-dimensional oscillator systems. *Phys. Rep.* **52**, 263–379.

Christou, A. A. 2000. A numerical survey of transient co-orbitals of the terrestrial planets. *Icarus* **144**, 1–20.

de la Barre, C. M., W. M. Kaula, and F. Varadi 1996. A study of orbits near Saturn's triangular Lagrangian points. *Icarus* **121**, 88–113.

Everhart, E. 1973. Horseshoe and Trojan orbits associated with Jupiter and Saturn. *Astron. J.* **78**, 316–328.

Fernandez, J. A., and W.-H. Ip 1984. Some dynamical aspects of the accretion of Uranus and Neptune—The exchange of orbital angular momentum with planetesimals. *Icarus* **58**, 109–120.

Fleming, H. J., and D. P. Hamilton 2000. On the origin of the Trojan asteroids: Effects of Jupiter's mass accretion and radial migration. *Icarus* **148**, 479–493.

Gladman, B. J., P. D. Nicholson, J. A. Burns, J. J. Kavelaars, B. G. Marsden, G. V. Williams, and W. B. Offutt 1998a. Discovery of two distant irregular moons of Uranus. *Nature* **392**, 897–899.

Gladman, B., J. J. Kavelaars, P. D. Nicholson, T. J. Loredo, and J. A. Burns 1998b. Pencil-beam surveys for faint trans-neptunian objects. *Astron. J.* **116**, 2042–2054.

Gladman, B., J. Kavelaars, M. Holman, J.-M. Petit, H. Scholl, P. Nicholson, and J. A. Burns 2000. The discovery of Uranus XIX, XX, and XXI. *Icarus* **147**, 320–324. Erratum in *Icarus* **148**, 302.

Gladman, B., J. J. Kavelaars, J. Petit, A. Morbidelli, M. J. Holman, and T. Loredo 2001. The structure of the Kuiper Belt: Size distribution and radial extent. *Astron. J.* **122**, 1051–1066.

Gomes, R. S. 1998. Dynamical effects of planetary migration on primordial Trojan-type asteroids. *Astron. J.* **116**, 2590–2597.

Hahn, J. M., and R. Malhotra 1999. Orbital evolution of planets embedded in a planetesimal disk. *Astron. J.* **117**, 3041–3053.

Holman, M. J. 1997. A possible long-lived belt of objects between Uranus and Neptune. *Nature* **387**, 785–788.

Holman, M. J., and J. Wisdom 1993. Dynamical stability in the outer Solar System and the delivery of short period comets. *Astron. J.* **105**, 1987–1999.

Holman, M. J., J. J. Kavelaars, B. J. Gladman, J.-M. Petit, D. Milisavljevic, and P. D. Nicholson 2001. Deep Optical Searches for Faint Uranian and Neptunian Satellites. *Bull. Am. Astron. Soc., 1108* **33**, [abstract #37.11.]

Ida, S., and J. Makino 1992. *N*-body simulation of gravitational interaction between planetesimals and a protoplanet. *Icarus* **96**, 107–120.

Innanen, K. A., and S. Mikkola 1989. Studies on Solar System dynamics. I—The stability of saturnian Trojans. *Astron. J.* **97**, 900–908.

Jedicke, R., J. Larsen, and T. Spahr 2002. Observational selection effects in asteroid surveys and estimates of asteroid population sizes. In *Asteroids III* (W. Bottke, A. Cellino, P. Paolicchi, and R. P. Binzel, Eds.). Univ. of Arizona Press, Tucson, in press.

Jewitt, D. C., C. A. Trujillo, and J. X. Luu 2000. Population and size distribution of small jovian Trojan asteroids. *Astron. J.* **120**, 1140–1147.

Levison, H. F., and M. Duncan 1994. The long term dynamical behavior of short period comets. *Icarus* **108**, 18–36. Also see http://www.boulder.swri.edu/~hal/swift.html.

Levison, H. F., and G. R. Stewart 2001. Remarks on modeling the formation of Uranus and Neptune. *Icarus* **153**, 224–228.

Levison, H. F., E. M. Shoemaker, and C. S. Shoemaker 1997. The long-term dynamical stability of Jupiter's Trojan asteroids. *Nature* **385**, 42–44.

Marzari, F., and H. Scholl 1998. Capture of Trojans by growing proto-Jupiter. *Icarus* **131**, 41–51.

Marzari, F., and H. Scholl 2000. The role of secular resonances in the history of Trojans. *Icarus* **146**, 232–239.

Marzari, F., H. Scholl, and P. Farinella 1996. Collision rates and impact velocities in the Trojan asteroid swarms. *Icarus* **119**, 192–201.

Marzari, F., P. Farinella, D. R. Davis, H. Scholl, and V. Campo Bagatin 1997. Collisional evolution of Trojan asteroids. *Icarus* **125**, 39–49.

Marzari, F., H. Scholl, C. Murray, and C. I. Lagerkvist 2002. Origin and evolution of Trojan asteroids. In *Asteroids III* (W. Bottke, A. Cellino, P. Paolicchi, and R. Binzel, Eds.). Univ. of Arizona Press, Tucson, in press.

Melita, M. D., and A. Brunini 2001. A possible long lived asteroid population at the equilateral Lagrangian points of Saturn. *Mon. Not. R. Astron. Soc.* **322**, L17–21.

Michtchenko, T. A., C. Beaugé, and F. Roig 2001. Planetary migration and the effects of mean motion resonances on Jupiter's Trojan asteroids. *Astron. J.* **122**, 3485–3491.

Mikkola, S., and K. Innanen 1992. A numerical exploration of the evolution of Trojan-type asteroidal orbits. *Astron. J.* **104**, 1641–1649.

Mikkola, S., K. Innanen, K. Muinonen, and E. Bowell 1994. A preliminary analysis of the orbit of the Mars Trojan asteroid (5261) Eureka. *Celest. Mech. Dynam. Astron.* **58**, 53–64.

Moons, M. 1993. *On the Resonant Hamiltonian in the Restricted Three-Body Problem*. Report 93-19, Department of Mathematics, Facultés Universitaires Notre Dame de la Paix, B-5000 Namur, Belgium.

Morbidelli, A. 2002. *Modern Celestial Mechanics. Aspects of Solar System Dynamics.* Taylor and Francis, London.

Morbidelli, A., and D. Nesvorný 1999. Numerous weak resonances drive asteroids toward terrestrial planets orbits. *Icarus* **139**, 295–308.

Namouni, F. 1999. Secular interactions of coorbiting objects. *Icarus* **137**, 293–314.

Nesvorný, D., and F. Roig 2000. Mean motion resonances in the trans-neptunian region. I. The 2 : 3 resonance with Neptune. *Icarus* **148**, 282–300.

Nesvorný, D., F. Thomas, S. Ferraz-Mello, and A. Morbidelli 2002. A perturbative treatment of the co-orbital motion. *Celest. Mech. Dynam. Astron.* **82**, 323–361.

Oseledec, V. I. 1968. A multiplicative ergodic theorem. Lyapunov characteristic numbers for dynamical systems. *Trans. Moscow Math. Soc.* **19**, 197–231.

Petit, J., A. Morbidelli, and G. B. Valsecchi 1999. Large scattered planetesimals and the excitation of the small body belts. *Icarus* **141**, 367–387.

Pollack, J. B., O. Hubickyj, P. Bodenheimer, J. J. Lissauer, M. Podolak, and Y. Greenzweig 1996. Formation of the giant planets by concurrent accretion of solids and gas. *Icarus* **124**, 62–85.

Quinlan, G. D., and S. Tremaine 1990. Symmetric multistep methods for the numerical integration of planetary orbits. *Astron. J.* **100**, 1694–1700.

Shoemaker, E. M., C. S. Shoemaker, and R. F. Wolfe 1989. Trojan asteroids—Populations, dynamical structure and origin of the L4 and L5 swarms. In *Asteroids II* (R. P. Binzel, T. Gehrels, and M. S. Matthews, Eds.), pp. 487–523. Univ. of Arizona Press, Tucson.

Storrs, A., B. Weiss, B. Zellner, W. Burleson, R. Sichitiu, E. Wells, C. Kowal, and D. Tholen 1999. Imaging observations of asteroids with Hubble Space Telescope. *Icarus* **137**, 260–268.

Thommes, E. W. T., M. J. Duncan, and H. F. Levison 1999. The formation of Uranus and Neptune in the Jupiter–Saturn region of the Solar System. *Nature* **402**, 635–637.

Thommes, E. W., M. J. Duncan, and H. F. Levison 2002. The formation of Uranus and Neptune among Jupiter and Saturn. *Astron. J.* **123**, 2862–2883.

Trujillo, C. A., D. C. Jewitt, and J. X. Luu 2001. Properties of the trans-neptunian belt: Statistics from the Canada–France–Hawaii Telescope survey. *Astron. J.* **122**, 457–473.

Weissman, P. R., and H. F. Levison 1997. The population of the trans-neptunian region: The Pluto–Charon environment. In *Pluto and Charon* (S. A. Stern and D. J. Tholen, Eds.), pp. 559–604. Univ. of Arizona Press, Tucson.

Wiegert, P. A., K. A. Innanen, and S. Mikkola 1997. An asteroidal companion to the Earth. *Nature* **387**, 685–685.

Wisdom, J. 1980. The resonance overlap criterion and the onset of stochastic behavior in the restricted three-body problem. *Astron. J.* **85**, 1122–1133.

Wisdom, J., and M. Holman 1991. Symplectic maps for the N-body problem. *Astron. J.* **102**, 1528–1538.

Wisdom, J., and M. Holman 1992. Symplectic maps for the N-body problem—Stability analysis. *Astron. J.* **104**, 2022–2029.

Yoder, C. F. 1979. Notes on the origin of the Trojan asteroids. *Icarus* **40**, 341–344.